Summer circulation and water masses transport in Bransfield Strait, Antarctica: An evaluation of their response to combined effects of Southern Annular Mode and El Niño–Southern Oscillation

Brendon Yuri Damini[1,2,*], André L. Brum[1,2], Rob A. Hall[3], Tiago S. Dotto[4], José Luiz L. Azevedo[1,2], Karen J. Heywood[3], Mauricio M. Mata[1,2], Carlos A. E. Garcia[1,2], Rodrigo Kerr[1,2,*]

[1]Laboratório de Estudos dos Oceanos e Clima – LEOC, Instituto de Oceanografia, Universidade Federal do Rio Grande – FURG, Av. Itália km 8, s/n, Rio Grande, RS, 96203–900, Brazil.

[2]Programa de Pós-Graduação em Oceanologia, Instituto de Oceanografia, Universidade Federal do Rio Grande – FURG, Av. Itália km 8, s/n, Rio Grande, RS, 96203–900, Brazil.

[3]Centre for Ocean and Atmospheric Sciences, School of Environmental Sciences, University of East Anglia, Norwich, NR4 7TJ, UK.

[4]National Oceanography Centre, Southampton, SO14 3ZH, UK

*Corresponding authors

Address: CEOCEAN, Instituto de Oceanografia, Universidade Federal do Rio Grande – FURG, Av. Itália km 8 s/nº, Rio Grande, RS, Brazil, 96203-900.

E-Mail: brendon.oceano@furg.br
E-Mail: rodrigokerr@furg.br

Submitted to Deep-Sea Research Part I

Highlights

- Long–term summer circulation in Bransfield Strait is re–examined by multiple datasets.
- Part of Bransfield Current exits via the gap between King George and Clarence Islands.
- Climate modes influence modified Transitional Zonal Water with Bellingshausen influence (TBW) intrusions into the region.
- TBW advection into Bransfield Strait increased by 30% in SEI+ index conditions.

Abstract

Bransfield Strait, situated in the northern Antarctic Peninsula, is a critical area for studying the impacts of climate change. This complexity arises from the convergence of distinct water masses: Transitional Zonal Water with Weddell influence (TWW), and Transitional Zonal Water with Bellingshausen influence (TBW). This study aims to give a long–term description of Bransfield Strait circulation during austral summers through high-quality hydrographic data from 2003–2019, altimetry data and the global eddy–resolving ocean reanalysis product GLORYS12v1. Findings reveal a cyclonic ocean circulation pattern within Bransfield Strait, characterized by the northeastward Bransfield Current along the South Shetland Islands and extending to Elephant Island, and the southwestward Antarctic Coastal Current entering near 62.40ºS and 55.00ºW. GLORYS12v1 and altimetry datasets revealed that: part of the Bransfield Current leaves the eastern basin between King George and Clarence Islands and recirculation around the South Shetland Islands, and provides the first robust estimate over an extended period that TBW is transported between King George and Elephant Islands and feeds Bransfield Current. Our results highlight links between the strength of TBW transport and variability in climate modes, quantifying their magnitude and variability due to wind forcing modulation by combined effects of Southern Annular Mode and El Niño–Southern Oscillation indices (SEI). For instance, time-averaged years of SEI negative conditions reveal 0.10 Sv of TBW entering the Bransfield Strait between King George and Elephant Islands. On the other hand, under SEI positive conditions, the TBW transport increases to 0.31 Sv. These observed changes are crucial for advancing our understanding of regional circulation patterns and their underlying mechanisms, as they directly influence the physical and biogeochemical properties of the region.

Keywords: Antarctic Coastal Current; Brasfield Current; Circumpolar Deep Water; ENSO; Northern Antarctic Peninsula; SAM; Southern Ocean Circulation

1. Introduction

Bransfield Strait is a semi–closed region in the northern Antarctic Peninsula, situated between the South Shetland Islands and Antarctic Peninsula (Figure 1). It is considered a key area for studying the impacts of climate change due to its transitional environment connecting waters from the cold shelf regime of the northwestern Weddell Sea with the relatively warm oceanic regime of the Bellingshausen Sea [e.g., Wilson et al. 1999; Gordon et al. 2000; Heywood et al. 2004; Dotto et al. 2016; Kerr et al. 2018a; Damini et al. 2022].

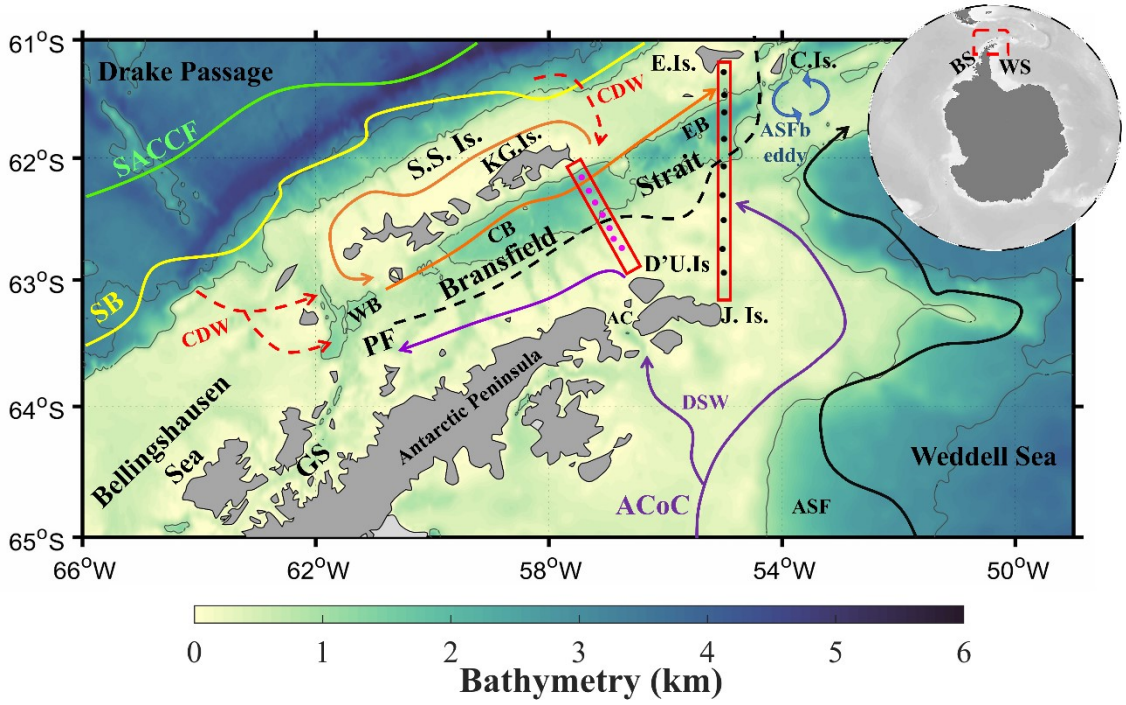

Figure. 1 Schematic representation of the mean circulation at the Northern Antarctic Peninsula. The red (purple) arrows represent the pathways of the Circumpolar Deep Water (Dense Shelf Water) entering Bransfield Strait. The green and yellow lines indicate the mean locations of the Southern Antarctic Circumpolar Current Front (SACCF) and Southern Boundary of Antarctic Circumpolar Current (SB), respectively. Light blue arrows indicate Antarctic Slope Front bifurcation (ASFb) eddy. The orange arrows depict Bransfield Current and its recirculation around the South Shetland Islands (S.S.Is.). The black line represents the mean location of the Antarctic Slope Front (ASF). The red rectangles bounding the magenta and black dots depict hydrographic Sections 1 and 2, respectively. The black dashed line represents the Peninsula Front (PF). The acronyms stand for: Antarctic Channel (AC), Antarctic Coastal Current (ACoC), Joinville Island (J.Is.), D'Urville Island (D'U.Is.), Elephant Island (E. Is.), Clarence Island (C. Is.), Bellingshausen Sea (BS), Drake Passage (DP), Weddell Sea (WS), Western Basin (WB), Central Basin (CB), Eastern Basin (EB), and Gerlache Strait (GS). The thin gray lines indicate the 0.10 km and 0.30 km isobaths provided by *https://www.scar.org/science/ibcso/ibcso/*. The inset panel depicts the region study. Modified from Damini et al. [2022].

In this context, several authors have reported significant changes in Bransfield Strait, particularly in the physical and biogeochemical of the water masses in the region [e.g., Dotto et al. 2016; Avelina et al. 2020; Ferreira et al. 2020; Damini et al. 2022; Santos-Andrade et al. 2023]. For instance, cooling, freshening, and lightening have been documented from the 1960s to 2000s [e.g., Wilson et al. 1999; Azaneu et al. 2013; Dotto et al. 2016; Ruiz Barlett et al. 2018; Damini et al. 2022], likely contributing to the dilution of total alkalinity and dissolved inorganic carbon concentration reported from 2000 to 2010 [Santos-Andrade et al. 2023]. However, since the 2010s, Bransfield Strait experienced signals of warming and salinification, which led to an increase in total alkalinity and dissolved inorganic carbon concentration [Dotto et al. 2016; Damini et al. 2022; Santos-Andrade et al. 2023]. This variability in water masses properties influences biological activity, such as phytoplankton succession [Mendes et al. 2018; Costa et al. 2020], and consequently affects the sea-air CO_2 exchanges in the region [Ito et al. 2018].

The circulation within Bransfield Strait comprises two main surface–subsurface currents: a northeastward jet, the Bransfield Current, which transports waters from the Bellingshausen Sea mixed with Circumpolar Deep Water – CDW (hereafter referred to as Transitional Zonal Water with Bellingshausen Sea influence – TBW) along the southern slope of the South Shetland Island; and the southwestward jet, the Antarctic Coastal Current, a coastally–trapped current which borders the northern slope of the Northern Antarctic Peninsula and advects Weddell Sea sourced waters (hereafter referred to as Transitional Zonal Water with Weddell Sea influence – TWW) [Fig. 1; e.g., Hofmann et al. 1996; von Gyldenfeldt et al. 2002; Heywood et al. 2004; Sangrà et al. 2011, 2017; Collares et al. 2018; van Caspel et al. 2018]. These boundary current jets are separated along Bransfield Strait by a surface thermal front known as the Peninsula Front (marked by the black dashed line in Figure 1). This shallow mesoscale structure is considered a crucial factor affecting regional

93 circulation, with its position modulated by the variability of water masses in Bransfield Strait
94 [Sangrà et al. 2011, 2017].

95 CDW is characterized by relatively warm, saline, low-oxygen, and nutrient and
96 carbon–rich intermediate waters advected by the Antarctic Circumpolar Current [ACC;
97 Martinson and McKee, 2012]. Along the western Antarctic Peninsula continental shelf, CDW
98 upwells to within 150–300 m of surface and mixes with waters from the Bellingshausen Sea,
99 forming the TBW [Orsi et al 1995], which subsequently intrudes into Bransfield Strait
100 [Gordon et al. 2000]. The primary pathways for TBW intrusions into Bransfield Strait are: (i)
101 between the South Shetland Islands, south of the western basin [Wessel an Smith, 1996], (ii)
102 south of Drake Passage between King George and Elephant Islands [Hofmann et al. 1996],
103 and (iii) through Gerlache Strait [Niller et al. 1991].

104 TWW is characterized by relatively cold and saline shelf waters advected by the
105 Antarctic Coastal Current from the Weddell Sea into Bransfield Strait via the Antarctic
106 Sound and at the north of Joinville Island [Gordon et al. 2000; Sangrà et al. 2011, 2017;
107 Collares et al. 2018]. Once it reaches Bransfield Strait, TWW sinks through several canyons
108 along the continental shelf [Lopez et al. 1999]. Furthermore, the topographic features of
109 Bransfield Strait facilitate the partitioning of the flow into three deep basins (western, central,
110 and eastern) separated by relatively shallow sills. These sills help preserve the thermohaline
111 properties of TWW in the deeper layer [Wilson et al. 1999], in its purest form in the central
112 basin [Dotto et al. 2016; Damini et al. 2022]. This makes Bransfield Strait an ideal proxy
113 region for studying the structure, variability, and trends of Weddell Sea shelf waters [Dotto et
114 al. 2016], an essential source of Antarctic Bottom Water [Kerr et al. 2018b].

115 The ACC plays a critical role in advecting CDW onto the Antarctic continental shelf,
116 contributing to the formation of TBW, which is subsequently transported into Bransfield

Strait. The ACC transport is concentrated in a series of well–defined fronts (i.e., Subantarctic Front, Polar Front, and Southern ACC Front – SACCF). Each of these fronts has distinct temperature and salinity gradients and their positions are influenced by wind pattern variability and associated climate modes [i.e., Southern Annular Mode – SAM and El Niño–Southern Oscillation – ENSO; Marshall et al. 2003; Renner et al. 2012]. In recent decades, the ACC fronts have migrated poleward [e.g., Yamazaki et al. 2021], which resulted in an increase in eddy kinetic energy [e.g., Hogg et al. 2015; Martínez-Moreno et al. 2022]. This poleward migration could lead to greater CDW inflow onto the Antarctic continental shelf, such as Bransfield Strait [e.g., Dotto et al. 2016; Damini et al. 2022; Ruiz Barllet et al. 2018] and/or could also promote the formation of eddies shed by the ACC towards the West Antarctic Peninsula [Martinson and McKee, 2012; Couto et al. 2017]. Moreover, the enhancement of CDW transport in these areas contributes to greater ice–mass loss due to the basal melt of ice shelves [Cook et al. 2016], leading to an increase in freshwater input to the ocean [Rott et al. 2018].

Observations have shown that the positive phase of SAM (SAM+) leads to an intensification and poleward shift of the westerly winds over the Southern Ocean [e.g., Thompson and Solomon, 2002], causing a poleward shift of SACCF [e.g., Yamazaki et al. 2021]. This is believed to intensify the intrusion of TBW [Ruiz Barlett et al. 2018] while weakening the inflow of TWW [Dotto et al. 2016; Damini et al. 2022] into Bransfield Strait. Conversely, the negative phase of SAM (SAM–) leads to a decrease and equatorward shift of the westerly winds over the Southern Ocean, causing an equatorward shift of SACCF, which intensifies the intrusion of TWW and weakens the inflow of TBW into Bransfield Strait [Marshal et al. 2003; Renner et al. 2012; Dotto et al. 2016; Damini et al. 2022]. Previous studies showed that the positive phase of ENSO (ENSO+) and negative phase of ENSO (ENSO–) induce similar circulation patterns to SAM– and SAM+, respectively [e.g., Yuan,

2004, 2018; Loeb et al. 2010; Ruiz Barlett et al. 2018]. Therefore, when both modes are in phase, i.e., during ENSO– and SAM+ or ENSO+ and SAM–, TBW advection into Bransfield Strait is intensified or weakened, respectively [e.g., Damini et al. 2022].

Although Bransfield Strait plays a crucial role in water mass exchange between the Bellingshausen and Weddell Seas [e.g., Gordon et al. 2000; Thompson et al. 2009], few studies have focused on its long–term circulation system and the temporal variability of water masses transport rates through this circulation system [Veny et al. 2022; Wang et al. 2022; Gordey et al. 2024]. This study re–examines the austral summer surface–subsurface circulation in Bransfield Strait using a long–term and high-quality hydrographic dataset spanning 2003 to 2019, provided by the Brazilian High Latitude Oceanography Group [GOAL; Mata et al. 2018]. The analysis also incorporates altimetry data and the global eddy-resolving ocean reanalysis product GLORYS12v1 [Jean-Michel et al. 2021]. In particular, we focus on the volume transport rates and temporal variability of water masses in the region under the combined effects of SAM and ENSO climate modes. Understanding the circulation in this dynamic region is crucial as it directly affects the physical processes, the distribution of biogeochemical properties and, consequently, the local biota and ecosystem connections.

2. Data and Methods

2.1. Hydrographic data

The hydrographic measurements were obtained during austral summers from 2003 to 2019 (Figure S1). During that period, two hydrographic sections in Bransfield Strait were occupied 17 times with ConductivityTemperature-Depth (CTD) profiles with 1 dbar of vertical resolution (Figure 1). Section 1 was located between King George and D'Urville Islands (indicated by a red rectangle bounding the magenta dots in Figure 1), while Section 2 was situated between Elephant and Joinville Islands (a red rectangle bounding the black dots

in Figure 1). The conservative temperature (Θ, ° C) and absolute salinity (S_A, g kg^{-1}) were computed using the International Thermodynamic Equation of Seawater – 2010 (TEOS – 10) [McDougall et al. 2009]. The reader is referred to Dotto et al. [2021] for more details about the GOAL hydrographic measurements used here.

2.2. Geostrophic velocities estimates by hydrographic data

Cross–section geostrophic ocean current velocities were computed, referencing the shear to a level of no motion at 500 m, following other studies carried out in this region [e.g., Grelowski et al. 1986; Gomis et al. 2002; Sangrà et al. 2011, 2017]. It seems that 500 m could be a good choice for the reference level, as only small areas of these sections extend beyond this depth. Additionally, the slope of the isopycnals at depths greater than 500 m is less pronounced (Figure S2), suggesting minimal contribution from deep layers to the upper geostrophic velocities. This choice therefore reduces the uncertainty associated with the selection of the no motion level. Furthermore, one of the main currents, the Bransfield Current, located along the edge of the South Shetland Islands is essentially confined to the upper 500 m (Figure 2). Mukhametyanov et al. [2022], tested different reference levels to calculate volume transports in the Bransfield Strait and compared their results with those obtained using a lowered current profiler. They reported that the 500 m reference level accounts for more than half of the lowered current profiler transport.

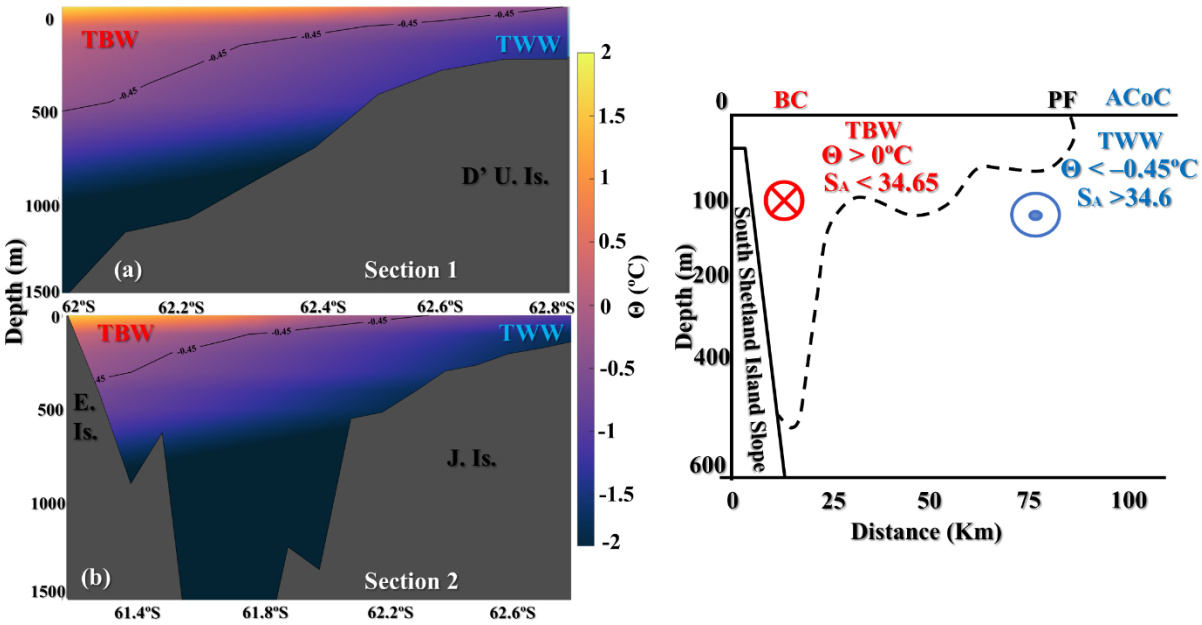

184

185 **Figure 2.** Time–averaged (2003–2019) of conservative temperature (Θ in ºC) within Bransfield Strait system
186 for **(a)** Section 1, between King George and D' Urville Island, and **(b)** Section 2 between Elephant and Joinvile
187 Islands. Scheme modified from Sangrà et al. [2011] of the main components of the Bransfield Strait system
188 along the section crossing of the strait (South Shetland Islands to Antarctic Peninsula) is depicted in **(c)**. The red
189 ⊗ indicates a flow into the page (i.e., northeastward flow), while the blue circle indicates a flow leaving the
190 page (i.e., southwestward flow). The acronyms stand for: Antarctic Coastal Current (ACoC), Bransfield Current
191 (BC), Transitional Zonal Water with Bellingshausen influence (TBW), Transitional Zonal Water with Weddell
192 influence (TWW), and Peninsula Front (PF). The topographic feature along the sections is shown in black and is
193 based on IBCSO v1.0 data (https://www.scar.org/science/ibcso/ibcso/).

194 The hydrographic properties (i.e., Θ and S_A) and geostrophic velocities along the
195 cross-sections were gridded onto 0.05º of latitude spanning from the first to the last
196 measurement profiles along each year's section. Each grid was 2–D interpolated using a
197 radial basis function with a linear weighting and the smoothing factor related to the
198 magnitude of signal noise, set to 0.1. The radial basis function interpolation method was
199 chosen for its flexibility in adapting to the spatial structure of the data, making it particularly
200 effective for irregular or sparse datasets. We decided to apply an interpolation method to
201 allow us to calculate the time–average over the entire period since we have spatial data gaps
202 in certain years.

2.3. Surface geostrophic circulation by satellite altimetry

The surface geostrophic circulation in the study area is derived from the Global Ocean Gridded L4 Sea Surface Heights and Derived Variables Reprocessed dataset (DOI:10.48670/moi-00145), accessible through the Copernicus Marine Environment Monitoring Service (CMEMS; data.marine.copernicus.eu). The surface geostrophic velocities derived from this dataset have a spatial resolution of 0.25º and were used for comparison with geostrophic velocities calculated from hydrography. Additionally, relative vorticity was calculated $\zeta_z = \partial v/\partial x - \partial u/\partial y$, where u and v are zonal and meridional components of the current velocity field, respectively.

2.4. Water mass transport calculation by GLORYS12v1 output

GLORYS12v1 is a global eddy-resolving physical ocean and sea ice reanalysis with 1/12º horizontal resolution and 50 standard vertical levels. It covers the period from 1993 to the present, is based on the Nucleos for European Modelling of the Ocean platform (NEMO), and is atmospherically forced with ERA–Interim (https://www.ecmwf.int/en/forecasts/dataset/ecmwf-reanalysis-interim). Quality assessments have shown that GLORYS12v1 effectively captures the main interannual climate variability signals for the ocean and sea ice [Jean-Michel et al. 2021]. Additionally, it effectively captures the low-frequency variability of the sea ice extent in the Arctic and Antarctic Oceans [Jean-Michel et al. 2021]. The GLORYS12v1 bathymetry is based on ETOPO1 for the deep ocean and GEBCO8 for the coast and continental shelf but does not include ice shelf cavities [Jean-Michel et al. 2021].

We select thermohaline properties and velocity field (i.e., with barotropic and baroclinic components) output from GLORYS12v1, corresponding to the same months as the hydrographic measurements. After that, we computed the Θ and S_A from GLORYS12v1

using the same methodology applied to the hydrographic dataset. Then, summer averages (January–March) of Θ, S_A and velocity were calculated. These averaged fields were used to estimate the volume transport of water masses (Sv; 1 Sv = 10^6 m^3 s^{-1}) across the mean positions of the two sections previously analyzed using hydrographic measurements. To achieve this, velocities perpendicular to each section were computed. Water mass transport across each section was computed by area–integrating the velocities within their respective layers, defined by Θ and S_A: Transitional Zonal Water with Bellingshausen influence (TBW, $\Theta > 0$ °C and $S_A < 34.65$ S_A, g kg^{-1}) and Transitional Zonal Water with Weddell influence (TWW, $\Theta < -0.45$°C and $S_A > 34.60$ S_A, g kg^{-1}), following criteria established in previous studies [e.g., Huneke et al. 2016; Morozov et al. 2021; Gordey et al. 2024]. To further investigate water mass transport variability in the northern Antarctic Peninsula, we computed the average thickness of CDW layer, defined by $\Theta > 0$ °C and 34.60 g $kg^{-1} < S_A > 34.92$ g kg^{-1}. This analysis reveals the vertical distribution of CDW and its influence on regional water mass circulation. It is worth mentioning that the use of higher-resolution models would likely lead to more accurate transport estimations, besides providing a better representation of small- and mesoscale processes. Such processes facilitate the upwelling of CDW onto the continental shelf [e.g., Moffat et al., 2009; Boeira Dias et al., 2023] and could affects the TBW transports into the Bransfield Strait. For instance, Ong et al. [2024], showed that eddy activity in cross-slope exchanges is significantly enhanced in models with resolutions higher than 1/20°.

The summer–averaged hydrographic measurements spanning the full study period (2003–2019) were utilized to validate GLORYS12v1 output. To achieve this, we gridded the hydrographic measurements onto the same grid of the reanalysis. Furthermore, for both datasets, the averaged thermohaline properties profile of the two analyzed sections were calculated to evaluate the difference between the datasets.

2.5. Ancillary data sets

The wind patterns around the Antarctic Peninsula, and consequently the circulation of Bransfield Strait (i.e., intrusion of TBW and TWW in the region), are influenced by both ENSO and SAM [e.g., Dotto et al. 2016; Ruiz Barlett et al. 2018; Damini et al. 2022]. In this study, we seek to understand the combined effects of summer SAM (https://legacy.bas.ac.uk/met/gjma/sam.html) and summer ENSO (https://origin.cpc.ncep.noaa.gov/products/analysis_monitoring/ensostuff/ONI_v5.php) on winds in the Antarctic Peninsula and their subsequent impact on Bransfield Strait's circulation. Therefore, we employed the summer SEI index (https://zenodo.org/records/7500163; Figure S3) to account for the combined effects of the SAM and ENSO indices. In summary, the indices SEI+ (values > 0.50) and SEI– (values < –0.50) represent combinations of SAM+ with ENSO– and SAM– with ENSO+ periods, respectively [for more details, please see Llanillo et al. 2023]. The average positions of SAACF during SEI+ and SEI– years conditions were derived from Argo float temperature profiles from 2004 to 2019 (https://sio-argo.ucsd.edu/RG_ Climatology.html) using the 1.80 ºC isotherm at 500 m [Orsi et al. 1995].

Following Veny et al. [2024], the average of the summertime (January–March) wind stress curl and Ekman vertical velocity were calculated from monthly averaged wind velocity from the European Centre for Medium–Range Weather Forecast Reanalysis – Interim [ERA – Interim; https://www.ecmwf.int/en/forecasts/dataset/ecmwf-reanalysis-interim; Dee et al. 2011], which has a horizontal resolution of 0.70 x 0.70º over the period 1979 to 2019. Anomalies of wind stress curl was calculated by subtracting the time–average over the full period (January–March, 2003–2019) from the average of each SEI period analyzed (i.e., SEI+ and SEI–). In addition, the Spearman's correlations between the normalized and

detrended wind stress curl over the northern Antarctica Peninsula and SEI indices were tested from 1979 to 2019.

3. Results and Discussion

3.1. The Bransfield Strait Circulation System in the Central and the Eastern Basin

3.1. 1. Subsurface circulation derived from hydrography

Bransfield Strait's circulation is characterized by a cyclonic circulation pattern consisting of two major inflows, namely the Bransfield Current and Antarctic Coastal Current, as depicted in the annual velocities (Figures 3 and 4) as well as time–averaged velocity field (i.e., mean of 14 years to section 1 and mean of 10 years to section 2; Figure 5a–d). The Bransfield Current, a northeastward flow, moves along the southern slope of the South Shetland Islands towards Elephant Island. The core of this flow has a time–averaged velocity of 10 ± 4 cm s^{-1} at the surface layer in Section 1, and 14 ± 2 cm s^{-1} at 100 m depth in Section 2 (Figures 5a–d). The velocities decrease towards the bottom at each section (Figures 5a–b). In contrast, the Antarctic Coastal Current is a southwestward flow along the northern slope of the northern Antarctic Peninsula. This flow reaches an average velocity of -5 ± 4 cm s^{-1} and -7 ± 2 cm s^{-1} at 100 m of depth in Sections 1 and 2, respectively (Figures 5a–d).

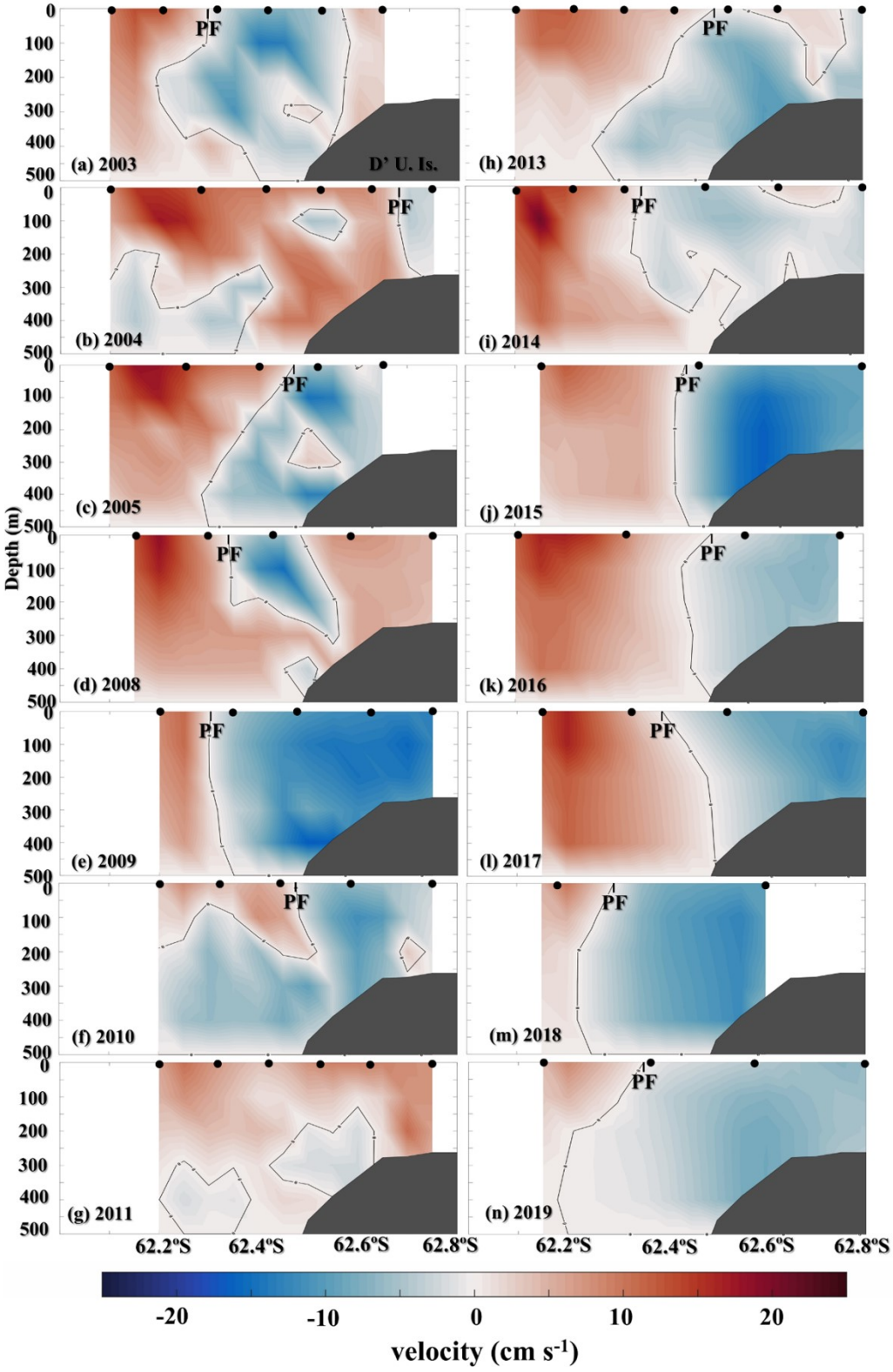

Figure 3. Annual cross–section geostrophic velocities at Section 1, between King George and D' Urville Islands (D' U. Is). Positive velocities correspond to Bransfield Current, while negative values indicate Antarctic Coastal Current. The thin black lines indicate the 0 m s^{-1} isolines of velocity. The position of the Peninsula Front (PF) is indicated by the black line on each panel. Black dots indicate the locations of the geostrophic current profiles. Topographic features along the sections are shown in black and are based on IBCSO v1.0 data (https://www.scar.org/science/ibcso/ibcso/).

299 At the surface, the boundary between the Bransfield Current and the Antarctic Coastal
300 Current depicts the Peninsula Front (black lines in Figures 3, 4 and 5). Previous studies,
301 based on summertime hydrographic measurements, have used different isotherms to
302 characterize the location of the Peninsula Front at the surface, ranging from –0.7˚C to 1˚C
303 [e.g., Sangrà et al. 2011, 2017; Huneke et al. 2016; Gordey et al. 2024]. Due to the variety of
304 definitions of the Peninsula Front, we opted to define it as the contour line where alongshore
305 surface geostrophic velocities are zero, which marks the switch in the ocean current direction.
306 In addition, using GLORYS12v1 outputs (which have no data spatial-temporal gaps during
307 summer–period of this study), we evaluated the long–term mean position of the Peninsula
308 Front and found close agreement in its averaged position based on the 0.5 ˚C isotherm and
309 the zero velocity definition (Figure S4).

310 The annual geostrophic velocity distributions (Figures 3 and 4) revealed interannual
311 displacement of the Peninsula Front across the hydrographic sections. This displacement
312 suggests temporal variability in the relative contributions of the Bransfield Current and the
313 Antarctic Coastal Current as also shown by temporal variability in the hydrographic
314 properties (i.e., Θ and $S_{A;}$ Figures S4, S5, S6 and S7) during the analyzed period. For
315 instance, in certain years (e.g., 2010, 2016 and 2019), a greater contribution of TWW was
316 inferred from lower Θ of the water column found along the sections (Figures S5, S6). This
317 situation is facilitated by the increased intensity of the Antarctic Coastal Current, which was
318 accompanied by a northward displacement of the Peninsula Front.

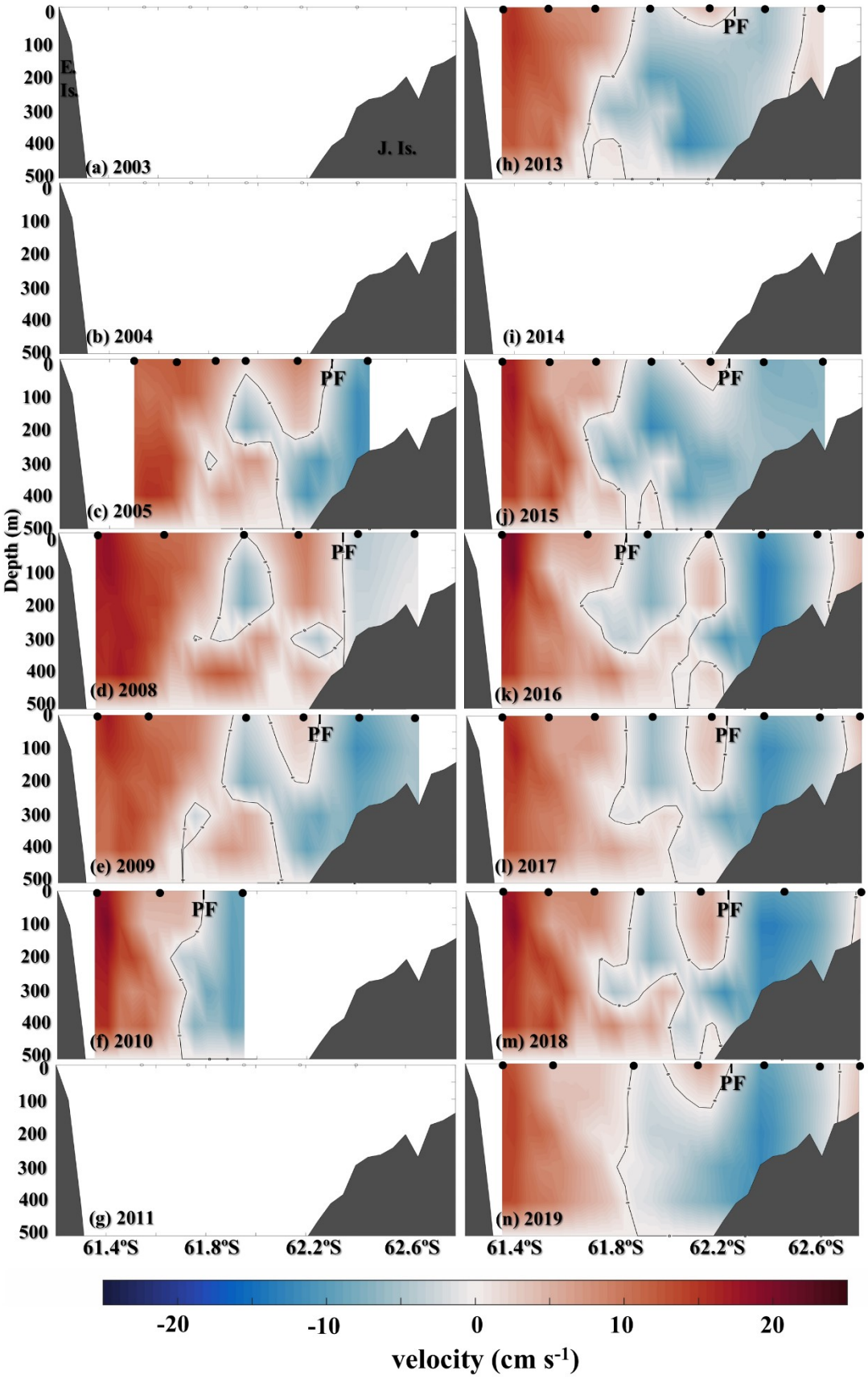

319

320 **Figure 4.** As Figure 3 but for section 2, between Elephant (E. Is.) and Joinville Islands (J. Is).

Thus, as reported in previous studies, the geostrophic estimates from hydrographic measurements along these two repeated sections revealed that the cyclonic circulation pattern in Bransfield Strait is primarily composed of surface–subsurface currents (i.e., the Bransfield and Antarctic Coastal Currents). Our further results suggest that the high interannual variability observed in hydrographic properties (i.e., Θ and S_A; Figures S5, S6, S7 and S8) is associated with changes in the intensification of these currents (Figures 3 and 4), as they are responsible for the advection of TBW and TWW within Bransfield Strait, respectively. For instance, years with a greater contribution of TWW within Bransfield Strait were associated with more intense of the Antarctic Coastal Current during those periods. Despite the cyclonic defined by these currents being well captured by geostrophic estimation from hydrographic measurements, we emphasize that the geostrophic approximation tends to underestimate compared to instantaneous directly-measured velocities (e.g. shipboard Acoustic Doppler Current Profiler observations) because (i) the latter also captures the influence of tides, inertial oscillations and wind–driven currents [Trasviña-Castro et al. 2011]; and (ii) the assumption of no motion at 500 m does not capture the barotropic component. Additionally, we emphasize that velocity fields are dependent on the spacing of stations. As such, cumulative volume transport estimates provide a more robust metric for discussion and comparison with previous studies, as they are not affected by variability in CTD station spacing occupation. However, given the presence of data gaps in certain years (Figure S1), we opted to calculate yearly water mass transports using velocities derived from the GLORYS12v1 output (**see section 3.2**). This approach ensures consistency and continuity in volume transport estimates throughout the study period.

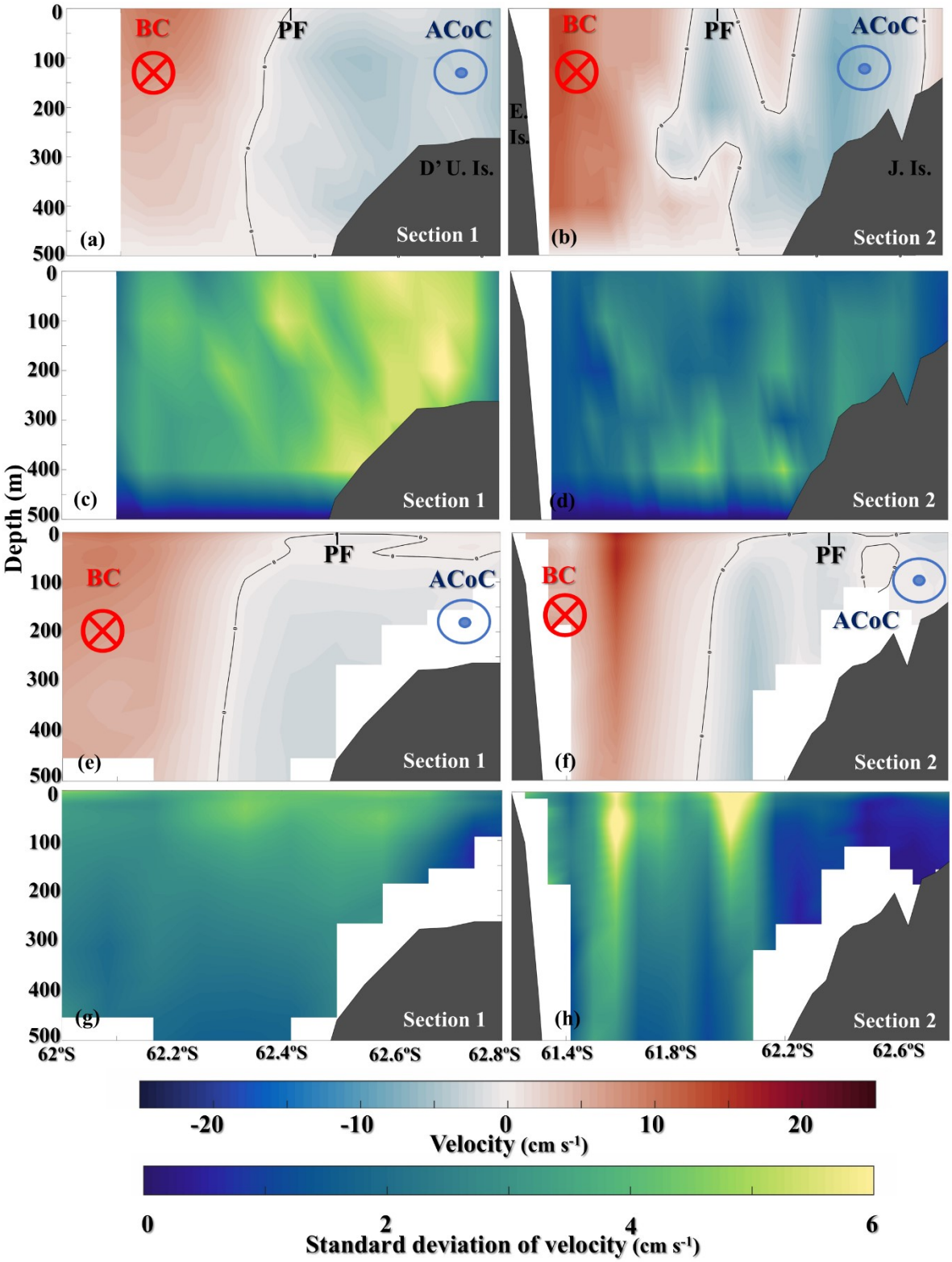

Figure 5. Time–averaged (2003–2019) of vertical cross–sections **(a)** of geostrophic velocities estimate from hydrographic measurements for the summertime (January–March) at Section 1, between King George and D' Urville Islands (D' U. Is.), and **(b)** Section 2, between Elephant (E. Is.) and Joinville Islands (J. Is.). Positive cross–sections velocities correspond to the Bransfield Current (BC), while negative values indicate the Antarctic Coastal Current (ACoC). The standard deviations of the geostrophic velocity time–averaged based hydrographic measurements are shown in panels **(c)** and **(d)** for sections 1 and 2, respectively. Similarly, the time–average of vertical cross–sections of velocities derived from GLORYS12v1 reanalysis product for the same period (i.e.,

January–March, 2003–2019) at **(e)** Section 1 and **(f)** Section 2. The corresponding standard deviations of the GLORYS's velocity time–averaged are shown in panels **(g)** and **(h)** for section 1 and 2, respectively. The red ⊗ indicates a flow into the page (i.e., northeastward flow), while the blue circle indicates a flow leaving the page (i.e., southwestward flow). The thin black lines indicate the 0 isolines of velocity. The position of the Peninsula Front (PF) is indicated by the black line on each panel. The topographic feature along the sections is shown in black and is based on IBCSO v1.0 data (https://www.scar.org/science/ibcso/ibcso/).

Overall, unlike previous studies that relied primarily on data from one or two oceanographic cruises [e.g., Sangrà et al., 2011, 2017; Gordey et al., 2024], this study is based on 17 years of observations, enabling a detailed analysis of long–term surface and subsurface circulation patterns in the Bransfield Strait, including the Bransfield Current and Antarctic Coastal Current. Thus, providing robust evidence of interannual variability in the intensity of these currents and consequently their influence on the hydrographic properties.

3.1. 2. Surface circulation derived from altimetry

We also analyze the surface geostrophic velocities derived from satellite altimetry, enabling the assessment of differences between the geostrophic velocity structure estimated from hydrographic measurements and the geostrophic velocity field derived from satellite estimates. Additionally, the altimetry estimates provide a broader perspective on geostrophic circulation, allowing the study of the velocity field across the entire region. Thus, by examining the time–averaged (January–March, 2003–2019) surface geostrophic velocities derived from satellite altimetry (Figure 6) we could observe the Bransfield Strait circulation patterns (i.e., Bransfield Current and Antarctic Coastal Current) similar to the geostrophic velocity estimates from the hydrographic measurements (Figures 3, 4 and 5a–b). The Bransfield Current is a coastal jet flowing northeastward along the southern slope of the South Shetland Islands extending towards Elephant Island (Figure 6). Previous studies have suggested that the Bransfield Current could extend as far as Elephant Island [e.g., López et al. 1999; Zhou et al. 2002, 2006; Thompson et al. 2009; Sángrà et al. 2011, 2017; Damini et al. 2023; Costa et al. 2023]. For instance, Thompson et al. [2009] observed, from drifter

trajectories, a continuation of the Bransfield Current near Clarence Island. Here we provide clear evidence from altimetry measurements to support these reports since we could observe the northeastward flow near Clarence Island, with time–averaged velocities of ~13 cm s^{-1} in Section 1 and ~16 cm s^{-1} in Section 2. The altimetry estimates (Figure 6) also corroborate previous studies regarding the dynamics of the Bransfield Current, showing that (i) part of the current leaves the eastern basin through the gap between King George and Clarence Islands, recirculating around the South Shetland Islands [López et al, 1999; Sangrà et al, 2011, 2017; Veny et al, 2024]; and (ii) part of the current in eastern Bransfield Strait basin is supplied by the intrusion of waters through the gap between King George and Elephant Islands [Hoffmann et al. 1996; López et al. 1999; Wilson et al. 1999; Loeb et al. 2009, 2010; Sanchez et al. 2019]. The Antarctic Coastal Current, a Northern Antarctic Peninsula slope–trapped current, is weaker with time–mean velocities of approximately –2 cm s^{-1} in both Sections 1 and 2 (Figure 6). The altimetry estimates indicate that the Antarctic Coastal Current enters Bransfield Strait at approximately 62.40ºS and 55.00ºW (Figure 6) in agreement with previous analysis of hydrographic sections [Heywood et al. 2004], moorings observations [von Gyldenfeldt et al. 2002] and trajectories of drifters [Thompson et al. 2009].

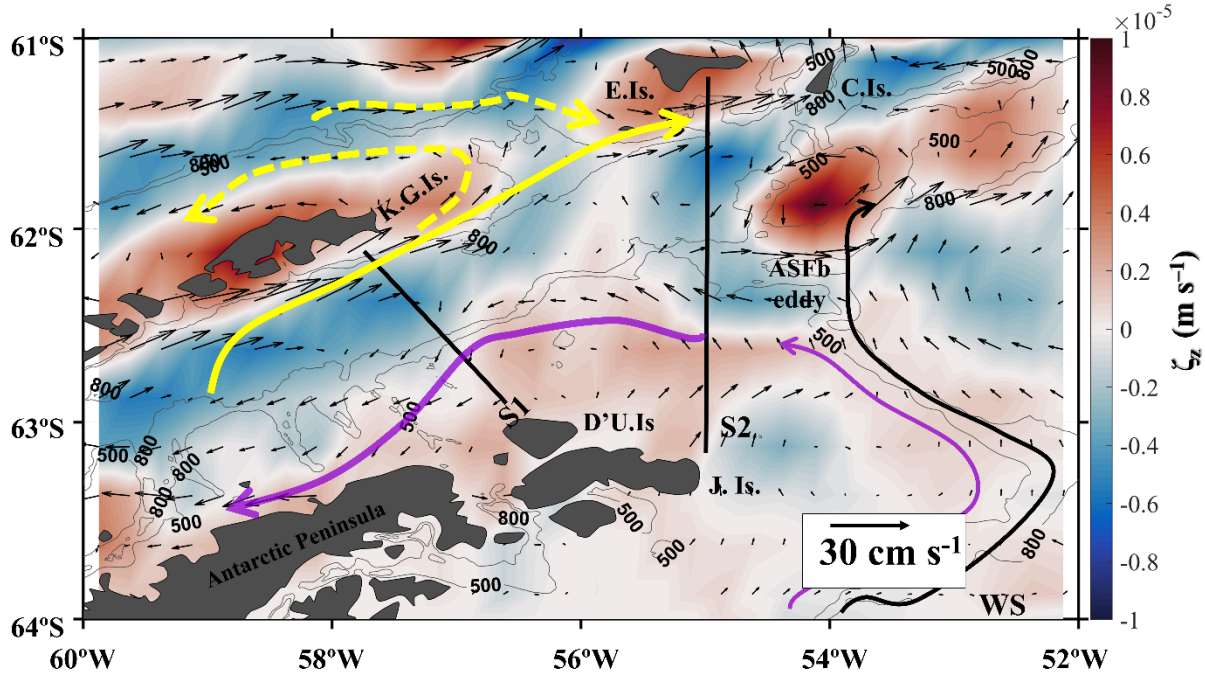

394

395 **Figure 6**. Time–averaged (January–March, 2003–2019) of relative vorticity (ζz; colour) and surface geostrophic
396 velocity (vectors) in the Northern Antarctica Peninsula derived from altimetry. The black lines represent the
397 mean position of the hydrographic Section 1 (S1) and Section 2 (S2) analyzed in this study. The yellow and
398 purple arrows represent Bransfield Current and Antarctic Coastal Current, respectively. The black arrow depicts
399 Antarctic Slope Front and ASFb eddy represents the Antarctic Slope Front bifurcation eddy. The acronyms
400 stand for: D'Urville Island (D'U.Is.), Clarence Island (C. Is.), Elephant Island (E. Is.), and Joinville Island
401 (J.Is.).The thin gray lines indicate the 500 m and 800 m isobaths based on IBCSO v1.0 data
402 (https://www.scar.org/science/ibcso/ibcso/).

403 The 17–year summer–mean surface circulation derived from altimetry reveals the
404 persistent presence of the Antarctic Slope Front bifurcation (ASF) eddy (Figure 6; Thompson
405 et al. 2009; Damini et al. 2023) trapped within the 500–800 m isobaths. The strong horizontal
406 velocity shear associated with the Antarctic Slope Front meandering likely forms and
407 maintains the ASFb above the topography due to potential vorticity conservation [Thompson
408 et al. 2009; Damini et al. 2023]. The presence of the ASFb eddy in the 17–year average
409 velocity field supports its persistent presence in the region, as previously demonstrated by
410 Thompson et al. [2009] using historical surface drifter data spanning from 1989 to 2005.
411 Additionally, some studies have shown that ASFb eddy play a crucial role in regulating sea–
412 air CO_2 exchanges, acting as a major region for CO_2 outgassing in the Bransfield Strait

413 [Damini et al. 2023; Kerr et al. 2025]. Therefore, indicating the importance of future studies
414 focusing on temporal investigations of this mesoscale structure.

415 Our satellite altimetry analysis provides robust evidence (with 17–year average
416 velocity field) of key circulation features in the Bransfield Strait, including the Bransfield and
417 Antarctic Coastal Currents, also ASFb eddy. Hence, corroborating previous studies based on
418 moorings and drifter measurements. These observations reinforce the findings from
419 hydrographic measurements, while the extended spatial coverage provided by altimetry
420 broadens our understanding of the regional circulation. The next section will explore the
421 implications of these circulation patterns for regional water masses transport (i.e., TBW and
422 TWW) within the Bransfield Strait and their variability.

423 **3.2. Water mass transport from the GLORYS12v1**

424 Few studies have focused on the interannual variability of water mass transports
425 within the Bransfield Strait and its drivers [e.g., Veny et al. 2022]. This study investigates the
426 interannual summer variability of TBW and TWW transport across two sections analysed
427 using hydrographic measurements and GLORYS12v1 outputs. Before calculating these
428 transports, we first validate GLORYS12v1 by comparing its outputs against hydrographic
429 properties and geostrophic transport estimates derived from hydrographic measurements
430 along the two sections examined in this study, thus ensuring the reliability of the reanalysis
431 product.

432 **3.2.1. Reanalysis validation**

433 A time–averaged (January–March, 2003–2019) comparison of the Θ and S_A mean
434 profile from the two sections derived from GLORYS12v1 outputs and available hydrographic
435 measurements, reveals some discrepancies. For instance, the Θ suggest a warm bias across

most of the vertical structure (Figure 7a), while the S_A profiles highlight a salty bias throughout much of the vertical S_A structure (Figure 7b). Despite these biases, GLORYS12v1 shows consistency in representing the main water masses advected by Bransfield Current and Antarctic Coastal Current (i.e., TBW and TWW, respectively; Figure 8).

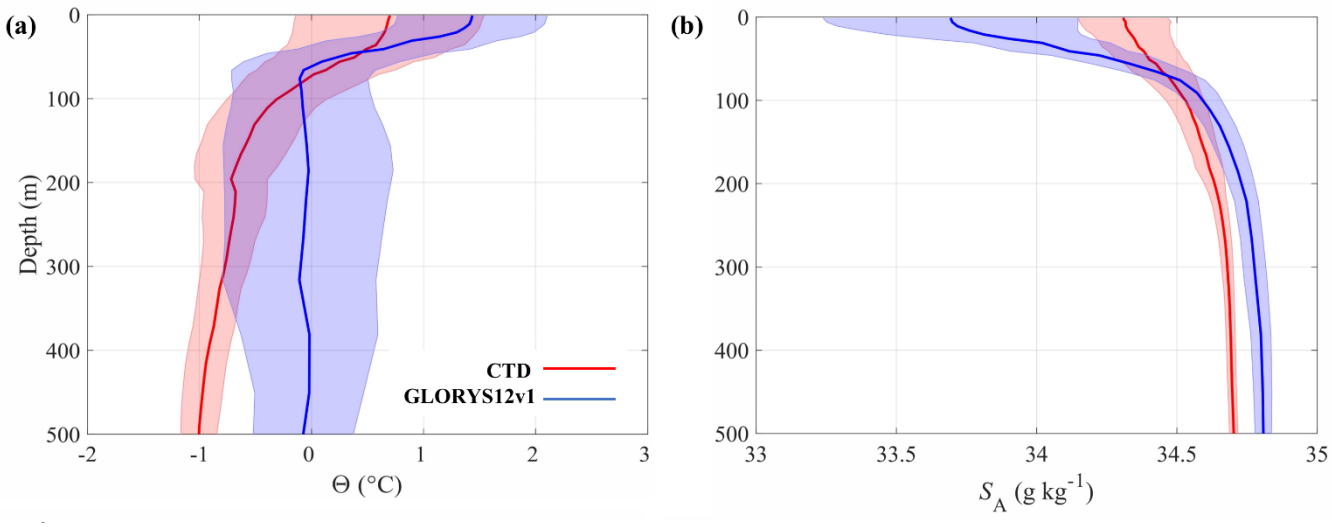

Figure 7. Time–averaged (January–March, 2003–2019) of the mean profile of **(a)** Θ and **(b)** S_A from the two sections by CTD dataset (in red) and GLORYS12v1 output (in blue), with the shaded area representing the standard deviation.

In addition, an analysis of the time–averaged cross–section velocities derived from the hydrographic measurements and GLORYS12v1 outputs indicates that both sections exhibited a cyclonic ocean circulation pattern (i.e., formed by the Bransfield Current and the Antarctic Coastal Current), consistent with our results estimates from hydrographic measurements (Figures 3 and 4). However, the GLORYS12v1 showed some discrepancies: (i) the Bransfield Current showed more intense in the GLORYS12v1 compared to hydrographic measurements, reaching a time–averaged velocity of 11 ± 4 cm s^{-1} and 18 ± 6 cm s^{-1} at the surface layer in Sections 1 and 2, respectively (Figure 5e–h); and (ii) the Antarctic Coastal Current showed weaker in GLORYS12v1 compared to estimates from hydrographic measurements, reaching a time–averaged velocity of –3 ± 2 cm s^{-1} at 453 m

depth in Sections 1 and –6 ± 3 cm s^{-1} at 380 m depth in Sections 2 (Figure 5e–h).

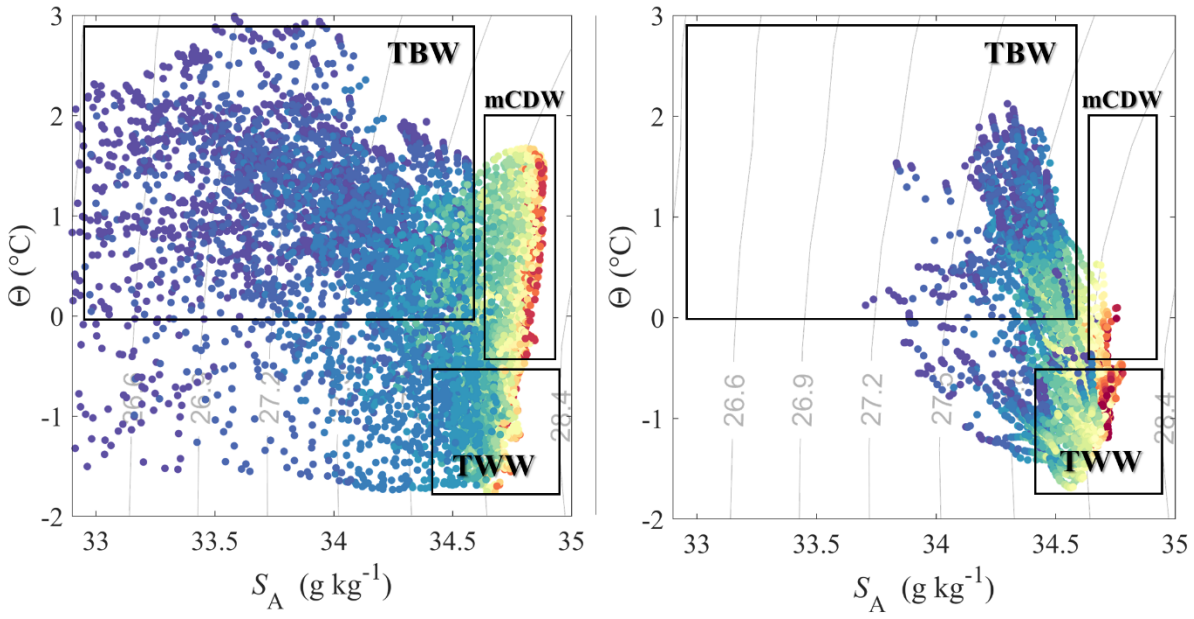

Figure 8. Summer–averaged (January–March) conservative temperature (Θ in ºC) – absolute salinity (S_A in g Kg^{-1}) diagrams up to 500 m depth for the two analyzed sections in the Bransfield Strait over the entire study period (2003–2019) for **(a)** GLORYS12v1 reanalysis and **(b)** CTD. The depth is indicated by the colours. The water masses indicated are: Transitional Zonal Water with Bellingshausen influence (TBW), Transitional Zonal Water with Weddell influence (TWW), and modifed Circumpolar Deep Water (mCDW). The boundaries of water masses indicated by black rectangles are based on [Huneke et al. 2016; Morozov et al. 2021; Gordey et al. 2024].

Since our focus is on study the variability of surface–subsurface currents (i.e., Bransfield Current and Antarctic Coastal Current), we calculated time–averaged (January–March, 2003–2019) of the depth-integrated (50–500 m) velocity field with the hydrographic properties (Θ and SA) averaged over depth (50–500 m) from GLORYS12v1. Thus, it reduces the high discrepancies observed in GLORYS12v1 at the surface (above 50 m; Figure 7) while allowing us to identify the circulation features in the Bransfield Strait, including the Bransfield Current and Antarctic Coastal Current, as well as the ASFb eddy. Our results show the influence of TBW (Figure 9) through a flow reaching ~ 0.50 ºC and ~ 34.45 g kg^{-1} at both sections (Figure 9). This flow is advected at ~ 12 cm s^{-1} by the Bransfield Current along the South Shetland Islands as far as Elephant Island (Figure 9c). This finding corroborates the altimetry estimates, which also evidenced that flow extends to Elephant

Island (Figure 6). Additionally, as seen in the altimetry measurements (Figure 6), there are distinct flows at the gap between King George and Elephant Islands, with an inflow near Elephant Island and an outflow near King George Islands (Figure 9). Conversely, as observed on time–averaged on the cross–section velocities (Figure 5e–f), an underestimation of the Antarctic Coastal Current within Bransfield Strait was observed in time–averaged of the depth–averaged field of properties (Figure 9). This discrepancy could be attributed to limitations in the bathymetry used in GLORYS12v1. Given the predominantly barotropic nature of this current [e.g., von Gyldenfeldt et al. 2002; Heywood et al. 2004], the Antarctic Coastal Current is particularly sensitive to local bathymetry. GLORYS12v1's bathymetry underestimates the depth of troughs in the region (Figure S9), potentially acting as a topography barrier and reducing the flow of the Antarctic Coastal Current into Bransfield Strait, thus affecting the circulation pattern of the region. Oelerich et al. [2022] reported similar findings in the Bellingshausen Sea, where GLORYS12v1 bathymetry restricts heat transport onto the continental shelf. Moreover, GLORYS12v1 does not capture the influence of the ASFb eddy, which is formed by the interaction between currents associated with the Antarctic Slope Front with the region's bathymetry. This likely stems from the underrepresentation of these currents or limitations in the reanalysis's bathymetry, which may not resolve the eddy's formation or trapping.

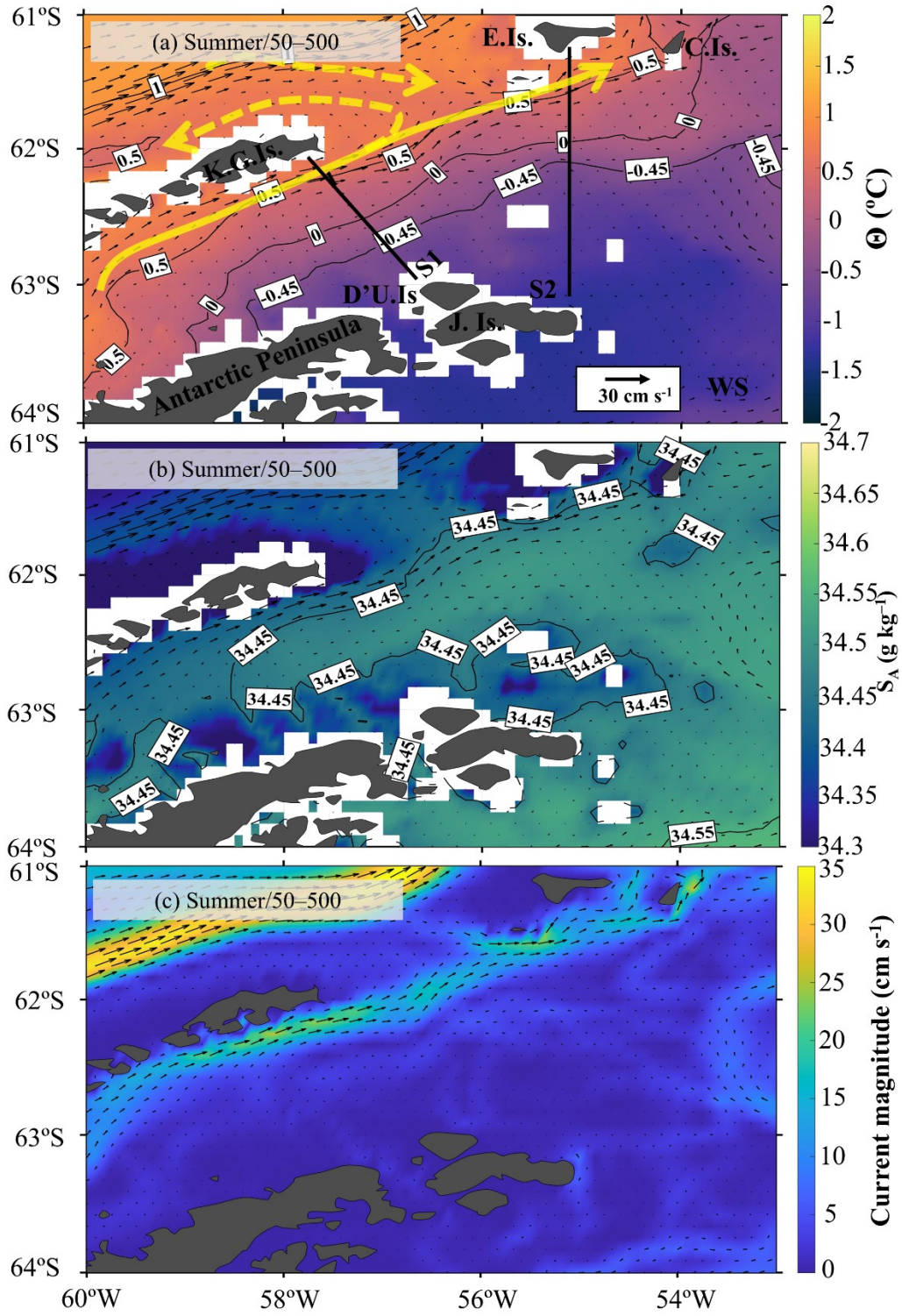

Figure 9. Time–mean of depth-integrated (50–500 m) velocity field (January–March, 2003–2019) with hydrographic properties averaged over the same depth range as the background field (colour) in the Northern Antarctic Peninsula, derived from GLORYS12v1 for **(a)** conservative temperature (Θ in ºC); **(b)** absolute salinity (S_A in g kg^{-1}) and **(c)** the current magnitude (cm s^{-1}) calculated as $\sqrt{u^2 + v^2}$ where u and v are the zonal and meridional velocity components, respectively. The black lines indicate the mean of positions of hydrographic sections 1 (S1) and 2 (S2) analyzed in this study. The yellow arrows represent the Bransfield Current. The acronyms stand for D'Urville Island (D'U.Is.), Clarence Island (C. Is.), Elephant Island (E. Is.), and Joinville Island (J.Is.).

The GLORYS12v1 demonstrated consistency with both altimetry and hydrographic measurements, underscoring its utility in capturing key features of the Bransfield Strait, including the cyclonic circulation formed by the Bransfield and Antarctic Coastal Currents, as well as the main water masses (i.e., TBW and TWW) transported by these currents, with the majority of their transport occurring within the upper 500 m (Figure 8). However, we suggest that inaccuracies in the model's bathymetry contribute to the observed underestimation of the Antarctic Coastal Current and limit its ability to fully resolve the ASFb eddy. Although these limitations warrant cautious interpretation, GLORYS12v1 remains a valuable tool to investigate water mass transport variability and the mechanisms driving this variability, particularly the influence of climate modes such as SAM and ENSO, which play a major role in modulating the regional dynamics and influence the biogeochemistry of the northern Antarctic Peninsula [e.g., Dotto et al. 2016; Avelina et al. 2020; Damini et al. 2022; Monteiro et al. 2023; Kerr et al. 2025].

3.2.2. Water masses transport and their variability

Here, we remind the reader that this study aims to investigate the summer variability of surface–subsurface currents within Bransfield Strait. In addition, as observed in the vertical resolution of velocities from GLORYS12v1 outputs (Figure S10), the troughs in Bransfield Strait represented by GLORYS12v1's bathymetry are shallower compared to available regional bathymetry datasets (e.g., IBCSO; Figure S9). Consequently, GLORYS12v1 contains only a few regions with depths greater than 500 m that include velocities outputs. Thus, we calculate the volume of water mass transports following their hydrographic properties (**see section 2.4**) up to 500 m depth. By the time–average (January–March, 2003–2019) of TBW volume transport via Bransfield Current estimated from GLORYS12v1 is 0.34 ± 0.24 Sv in Section 1 and 0.53 ± 0.34 Sv in Section 2 (Figure 10).

Assuming mass conservation, we infer an intrusion of TBW into the eastern basin of Bransfield Strait through the gap between King George and Elephant Islands, with a time–average of 0.23 ± 0.20 Sv (Figure 10). This intrusion is likely fed by CDW upwelling to depths of 150–300 m as ACC reaches Drake Passage [Orsi et al. 1995]. Our findings suggest this upwelling is driven by a pronounced negative wind stress curl in the region (Figure 10), which generates surface water divergence and brings CDW to shallow depths (~190 m; Figure S11a) via Ekman suction. After TBW enters the eastern basin of Bransfield Strait, this water flows eastward, driven by Bransfield Current towards the Powell Basin. Additionally, our results agree with previous studies, which reported geostrophic estimates (50–500 m) of summertime (January–March) volume transport ranging between 0.38 and 1 Sv for the Bransfield Current along the South Shetland Islands, [López et al. 1999; Sangrà et al. 2011]. On the other hand, despite GLORYS12v1 underestimates the Antarctic Coastal Current (Figure 5e–f), we found a time–average of TWW volume transport of approximately –0.09 ± 0.11 Sv and –0.02 ± 0.11 Sv through Sections 1 and 2, respectively (Figure 10). Sangrà et al. [2011], reported summertime (January–March) geostrophic estimates (0–500 m) of volume transport from two cruises of around –0.20 ± 0.10 Sv for the Antarctic Coastal Current near D' Urville Island.

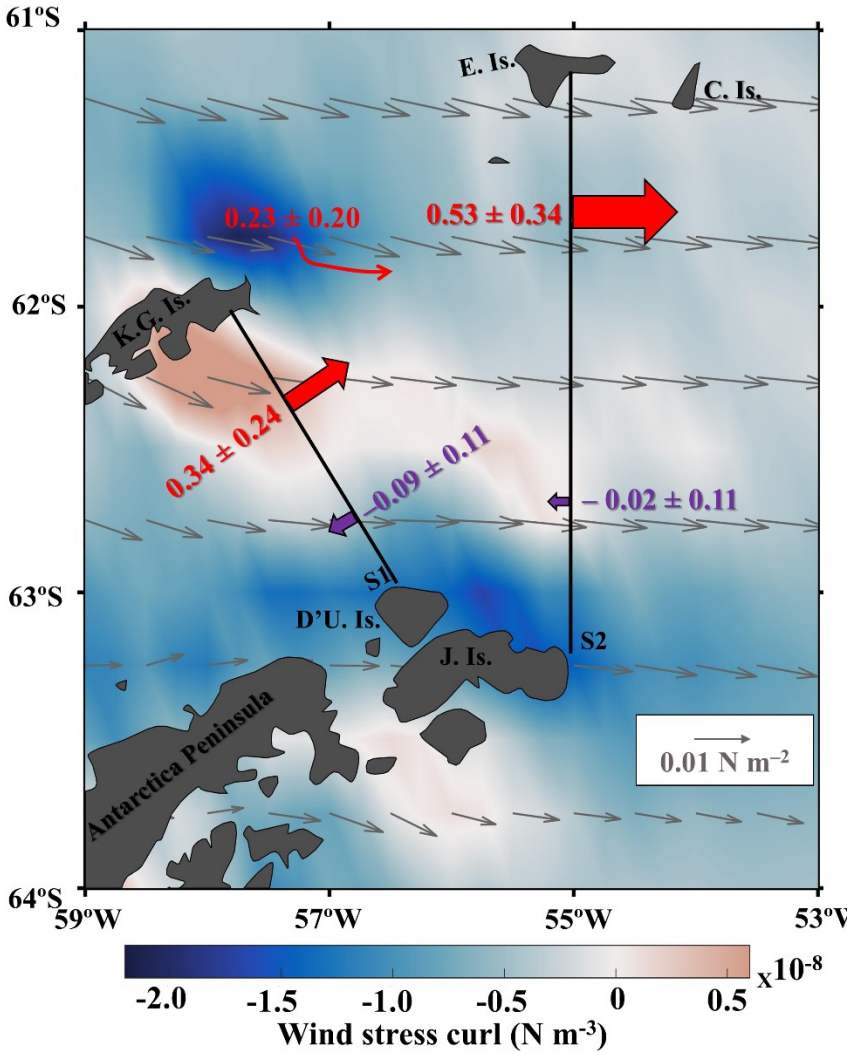

543

544 **Figure 10.** Surface horizontal distribution of time–averaged (January–March, 2003–2019) wind stress curl
545 (colour–coded), with purple and red solid arrows representing the time-averaged volume transport (Sv) of
546 Transitional Zonal Water with Weddell influence (TWW) and Transitional Zonal Water with Bellingshausen
547 influence (TBW), respectively. The mean position of Sections 1 (S1) and 2 (S2) are depicted as black solid
548 lines. Additionally, the length of the arrows indicates the magnitude of these transports. The grey vectors depict
549 the wind stress. The acronyms stand for: D'Urville Island (D'U.Is.), Clarence Island (C. Is.), Elephant Island (E.
550 Is.), and Joinville Island (J.Is.).

551 Overall, our results provide a valuable estimate for the intrusion of TBW into the
552 Bransfield Strait through the gap between King George and Elephant Islands. This intrusion
553 is influenced by the local wind patterns of the region, further emphasizing the dynamic of the
554 region's circulation and the importance of understanding these interannual variability in the
555 context of global climate change. Additionally, the good representation of TBW in
556 GLORYS12v1 reanalysis output (Figure 8) and the effective representation of the Bransfield

Current through velocity fields (Figures 5e–f and 9) suggest that the reanalysis can reliably capture the variability in TBW volume transport via the Bransfield Current. However, due to the reanalysis's bathymetry inaccuracies, an underestimation of the Antarctic Coastal Current limits the GLORYS's ability to fully resolve the TWW transport, resulting in low TWW volume transport values (Figure 10). Consequently, we could only evaluate the variability of TBW transport associated with the summer SEI indices.

We highlight that the use of the SEI index provides a more comprehensive understanding of how SAM and ENSO jointly modulate wind–driven circulation dynamics in the region. For instance, Llanillo et al. [2023] reported a stronger correlation when considering the SEI index rather than individual climate modes to explain the variability of intrusions of the Warm Deep Water (modified CDW in the Weddell Sea) onto the continental shelf. Furthermore, using monthly averaged wind velocity (Jan–March, 2003–2019) provides by ERA–Interim we calculated wind speed by $| V |= \sqrt{u^2 + v^2}$ (where u and v are the zonal and meridional wind velocity components, respectively) for each summer climate mode period, such as ENSO+ (2004, 2005, 2010, 2015, 2016), ENSO–+ (2006, 2008, 2009, 2011, 2012, 2018, 2019), SAM+ (2005, 2008, 2009, 2012, 2013, 2014, 2015, 2016, 2018, 2019), SAM– (2003, 2010, 2017), SEI+ (2006, 2008, 2009, 2011, 2012, 2013, 2015, 2018) and SEI– (2004, 2005, 2010, 2016, 2019) over the northern Antarctic Peninsula (~61–66ºS and 66–52ºW). Our results indicate that SEI periods lead to more intense winds, with an average wind speed of 3.15 ± 0.53 m s^{-1} during SEI+ phases and 3.74 ± 0.89 m s^{-1} during SEI– phases. In comparison, SAM+ (SAM–) periods showed an average wind speed of 2.86 ± 0.50 m s^{-1} (3.00 ± 0.81 m s^{-1}), while ENSO+ (ENSO–) periods exhibited an average wind speed of 2.75 ± 0.52 m s^{-1} (3.00 ± 0.55 m s^{-1}). Thus, underscoring the importance of considering both climate modes in the dynamic circulation studies in the Antarctic regions. The Spearman's correlations between the normalized and detrended Wind Stress Curl and SEI indices were

582 tested from 2003 to 2019 and showed a significant anti–correlation ($r = -0.60$ at the >95%
583 statistical significance level; Figure S3b). This result is in line with previous studies that
584 demonstrate the important role of SAM and ENSO climate modes in driving wind variability
585 in the region [e.g., Miguel Andres-Martin et al. 2024].

586 For the time–average of summers of SEI+ conditions (Figures 11a and S3a), stronger
587 northwesterly winds along the northern Antarctic Peninsula were observed (Figure S3b),
588 which, through Ekman transport, drives the SACCF closer to the Peninsula (Figure 11a).
589 These observations align with previous studies that have reported a poleward shift of SACCF
590 under similar wind patterns [e.g., Marshall et al. 2003; Loeb et al. 2009, 2010; Renner et al.
591 2012]. Additionally, this wind regime induces a pronounced negative wind stress curl over
592 the Antarctica Peninsula, as evidenced by positive wind stress curl anomalies (i.e., since that
593 the wind stress curl in the Antarctic Peninsula region is predominantly negative, SEI+ periods
594 exhibit more negative wind stress curl conditions compared to the overall temporal average;
595 Figure 11a). This shallow CDW (Figure S11b) might then be mixed with waters from the
596 Bellingshausen Sea, forming TBW, which is subsequently transported into the Bransfield
597 Strait through the gap between King George Island and Elephant Island (Figure S12a). This
598 TBW intrusion process is supported by an increase in TBW transport from 0.36 ± 0.20 Sv in
599 Section 1 to 0.71 ± 0.28 Sv in Section 2 during the average of SEI+ periods (Figure 11a), and
600 assuming mass conservation, we infer TBW volume transport through the gap between King
601 George Island and Elephant Island of 0.31 ± 0.16 Sv (Figure 11a). Our findings are coherent
602 with the changes in hydrographic (freshening and lightening) and biogeochemical (dilution of
603 total alkalinity and dissolved inorganic carbon) parameters as reported by Dotto et al. [2016],
604 Damini et al. [2022] and Santos-Andrade et al. [2023]. These authors hypothesized that
605 changes observed in Bransfield Strait are related to an increase in TBW volume transport into
606 Bransfield Strait associated with the intensification of westerly winds associated with climate

modes (i.e., SAM and ENSO events). Here we provide evidence from GLORYS12v1 to support that hypothesis.

For the time–average of summers of SEI– conditions (Figures 11b and S3a), weaker northwesterly winds and some southeasterly winds were observed (Figure S3c), through Ekman transport cause the SACCF to shift further away from the Antarctic Peninsula (Figure 11b). These observations also corroborate previous findings on the SACCF northward shifts under comparable wind patterns [e.g., Marshall et al. 2003; Loeb et al. 2009, 2010; Renner et al. 2012]. This wind pattern induces a weaker negative wind stress curl over the Antarctica Peninsula, evidenced by negative values on the wind stress curl anomaly (i.e., SEI– periods exhibit less negative wind stress curl conditions compared to the overall temporal average Figure 11b). The weaker wind stress curl over the Antarctica Peninsula (Figure 11b) leads to reduced Ekman transport of surface waters and reduced CDW upwelling (Figure S11c), which consequently decreases TBW advection into the Bransfield Strait (Figure S12b). This is consistent with the lower TBW volume transport observed during SEI– periods compared with SEI+ periods, with values of 0.27 ± 0.25 Sv in Section 1 and 0.33 ± 0.28 Sv in Section 2 (Figure 11b). Assuming mass conservation, we infer a TBW volume transport of 0.10 ± 0.03 Sv through the gap between King George and Elephant Islands during SEI+ summers. This represents a reduction of approximately 30% of TBW accessing the eastern Bransfield Strait through this gap during SEI– periods, compared to SEI+ periods (Figure 11b). Therefore, our results evidenced the interplay between TBW transport and climate modes (i.e., SEI index), emphasizing the sensitivity of Bransfield Strait circulation to atmospheric forces.

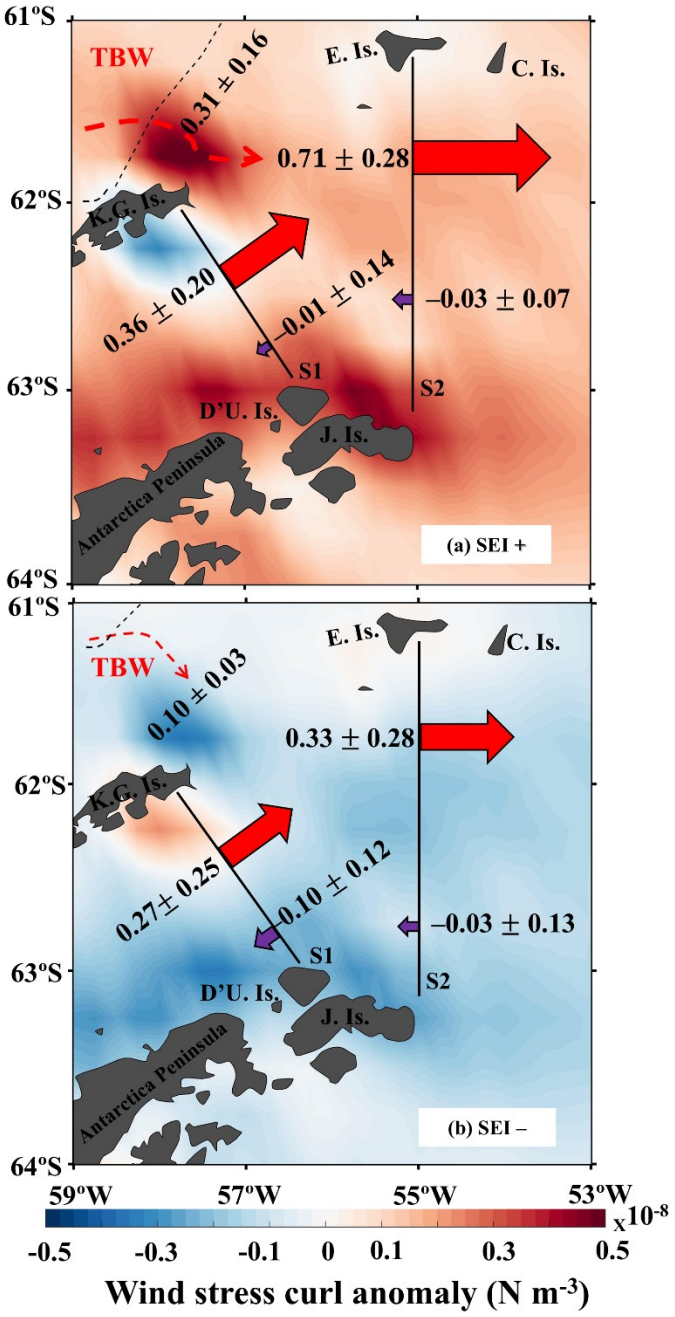

628

Figure 11. Surface horizontal distribution of averaged wind stress curl anomaly (colour–coded) of (a) SEI+ phase summers (i.e., 2006, 2008, 2009, 2011, 2012, 2013, 2014, 2015, and 2018) and (b) SEI– phase summers (i.e., 2010, 2016, and 2019). The purple and red solid arrows represent the time-averaged volume transport (Sv) of Transitional Zonal Water with Weddell influence (TWW) and Transitional Zonal Water with Bellingshausen influence (TBW), respectively, and their widths indicate the magnitude of these transports. The time-averaged of the TBW and TWW transports and the standard deviation of time-averaged are indicated by numbers. Southern Antarctic Circumpolar Current Front (SACCF) is represented by a black dashed line in both maps, while the mean position of Sections 1 (S1) and 2 (S2) are denoted by black solid lines. The acronyms stand for: D'Urville Island (D'U.Is.), Clarence Island (C. Is.), Elephant Island (E. Is.), and Joinville Island (J.Is.).

629 We highlight that additional factors in the Bransfield Strait, potentially unresolved by

630 the resolution of GLORYS12v1 (e.g., underestimation of the currents due to inaccuracies of

631 topography) may influence the interannual variability of TBW transport into Bransfield Strait
632 (Figure S9). For instance, unidentified processes may have intensified TBW outflow along
633 the 500 m isobath near King George Island in 2004, 2007, and 2017 (Figure S13a). In
634 addition, the absence of eddies representation because of GLORYS12v1's resolution could
635 affect the variability of TBW transport into Bransfield Strait as well. Those structures (i.e.,
636 eddies) facilitate the upwelling of CDW onto the continental shelf [e.g., Moffat et al. 2009;
637 Boeira Dias et al. 2023], contributing to the formation of TBW, which is subsequently
638 transported into the Bransfield Strait. Despite these limitations, our results confirm a strong
639 relationship between SEI influence on wind stress curl and TBW transport (Figures 11, S12,
640 S13 and S14), indicating that GLORYS12v1 provides a reliable basis for studying ocean
641 dynamics in Bransfield Strait. Nevertheless, further studies using higher-resolution models or
642 additional observational data are necessary to fully understand local dynamics.

643 A poleward shift of the SACCF has been observed associated with climate modes
644 [e.g., ENSO and SAM; Yuan, 2004; Loeb et al. 2009, 2010]. Here, we observed this shift for
645 the average of SEI+ summers (Figure 11a). This shift has significant implications for the
646 circulation and characteristics of Bransfield Strait. For example, poleward movement of
647 SACCF during SAM+ and/or ENSO– periods could bring warm, nutrient–rich CDW, which
648 mixes with iron-rich coastal waters, enhancing primary production [e.g., Loeb et al. 2009,
649 2010]. This process could lead to an increase in the consumption of organic matter in the
650 region and contribute to the formation of a CO_2 sink area [da Cunha et al. 2018; Avelina et al.
651 2020]. Our GLORYS12v1 analysis provides evidence of this CDW upwelling to shallow
652 depth (Figure S11) and supports these studies. Additionally, a tendency for more frequent
653 SAM+ and ENSO– periods in future has been reported in previous studies based on climate
654 model projections [e.g., Cai et al. 2015; Fogt and Marshall, 2020], that could potentially
655 leading a more frequent of that combined event occurs (referred to here as SEI+). And

consequently, leading to a greater intrusion of CDW into Bransfield Strait. These observations underscore the importance of comprehensively understanding regional circulation patterns and their driving mechanisms in a climate–sensitive polar environment.

Summary and conclusions

Here, we reported the first comprehensive long–term assessment of summer circulation within Bransfield Strait between 2003 and 2019, integrating high–quality hydrographic measurements, satellite altimetry, and the output of an eddy-permitting ocean reanalysis (GLORYS12v1). The geostrophic estimates from hydrographic measurements along the two repetitive sections used in this study show that the cyclonic circulation pattern in Bransfield Strait is primarily composed of the Bransfield and Antarctic Coastal Currents. Furthermore, our results reveal that the high interannual variability of hydrographic properties observed in the region is associated with changes in the intensification of these currents, which are responsible for the advection of TBW and TWW within Bransfield Strait. Both altimetry and reanalysis agree with the previous studies [e.g., López et al. 1999; Gordon et al. 2000; Loeb et al. 2009, 2010; Veny et al. 2024] highlighting the intrusion of TBW between King George and Elephant Islands feeding the Bransfield Current. The velocity fields from the GLORYS12v1 showed reasonable agreement with observations. For instance, the reanalysis accurately represents the influence of TBW and Bransfield Current system, highlighting the need for further efforts to address the representation of Weddell Sea currents, such as Antarctic Coastal Current and currents associated with Antarctic Slope Front, and their impact on the northern Antarctic Peninsula region. Our study suggests that, although absolute values may have some discrepancies, GLORYS12v1 provides a reliable basis for studying ocean dynamics in the northern Antarctic Peninsula.

Furthermore, by using GLORYS12v1 output we quantified the long–term TBW intrusions through the gap between King George and Elephant Islands, a key aspect of our study. We estimate a time–average rate of 0.23 ± 0.20 Sv from 2003 to 2019, providing the first robust estimate of this process over an extended period. While previous studies [e.g., López et al., 1999; Gordon et al., 2000; Loeb et al., 2009, 2010; Veny et al., 2024] have documented TBW intrusions into the Bransfield Strait, our study advances these findings by quantifying their magnitude and variability, indicating the wind forcing modulation by combined effects of SAM and ENSO. The averaged SEI+ summer conditions induce a pronounced negative wind stress curl over Antarctica Peninsula, resulting in ~ 30% increase in the inflow of TBW through the gap between King George and Elephant Islands. The long–term trends associated with the projected southward migration of the winds and ACC could favor more intrusion of TBW into the region. This would alter both physical and biogeochemical properties in the northern Antarctic Peninsula, with potential impacts on carbon sequestration and instability of regional glaciers. Given these potential impacts, ongoing hydrographic observations and assessing high–resolution ocean circulation models [e.g., Regional Ocean Modeling System – ROMS; Wang et al. 2022] are essential for further understanding of the regional circulation and its influence on water mass transport and biogeochemical processes.

Acknowledgements

This study is part of the activities of the Brazilian High Latitude Oceanography Group (GOAL) within the Brazilian Antarctic Program (PROANTAR). GOAL has been funded by and/or has received logistical support from the Brazilian Ministry of the Environment (MMA); the Brazilian Ministry of Science, Technology, and Innovation (MCTI); the Council for Research and Scientific Development of Brazil (CNPq); the Brazilian Navy; the Inter-

703 ministerial Secretariat for Sea Resources (SECIRM); the National Institute of Science and
704 Technology of the Cryosphere (INCT CRIOSFERA; CNPq Grant Nos. 573720/2008-8 and
705 465680/2014-3); and the Research Support Foundation of the State of Rio Grande do Sul
706 (FAPERGS Grant No. 17/2551-000518-0). This study was conducted within the activities of
707 the GOAL projects (CNPq Grant Nos. 550370/2002-1, 520189/2006-0, 556848/2009-8,
708 565040/2010-3, 405869/2013-4, 407889/2013-2, 442628/2018-8, 442637/2018-
709 7,440859/2023-9, and 440865/2023-9) and CARBON Team activities
710 (www.carbonteam.furg.br). Financial support was also received from Coordination for the
711 Improvement of Higher Education Personnel (CAPES) through the project CAPES “Ciências
712 do Mar” (grant no. 23038.001421/2014-30). CAPES also provided free access to many
713 relevant journals through the portal “Periódicos CAPES” and the activities of the Graduate
714 Program in Oceanology. For the purpose of open access, the author(s) has applied a Creative
715 Commons attribution (CC BY) licence to any Author Accepted Manuscript version arising.
716 Rodrigo Kerr and Mauricio M. Mata are granted researcher fellowships from CNPq Grant
717 Nos. 309978/2021-1 and 312569/2021-1, respectively. Brendon Yuri Damini acknowledges
718 financial support from CAPES PhD. scholarship Grant Nº. 88887.719848/2022-00 and
719 88881.982653/2024-01. Karen J Heywood and Rob A Hall were supported by Natural
720 Environment Research Council (NERC) Grant NE/P021395/1 and NE/S006419/1. Tiago S.
721 Dotto was supported by NERC National Capability programme AtlantiS (NE/Y005589/1).
722 The authors thank the officers and crew of the polar vessel *Almirante Maximiano* of the
723 Brazilian Navy, and the several scientists and technicians participating in the cruise for their
724 valuable help during data sampling and data processing. All datasets used and respective
725 websites are indicated in the manuscript. We are grateful for the constructive comments
726 provided by two anonymous reviewers, who substantially helped to improve the manuscript.

727

References

Avelina, R., Cotrim da Cunha, L., Farias, C.D.O., Hamacher, C., Kerr, R., Mata, M.M. (2020). Contrasting dissolved organic carbon concentrations in the Bransfield Strait, Northern Antarctic Peninsula: Insights into ENSO and SAM effects. Journal of Marine Systems, 103, 103457. https://doi.org/10.1016/j.jmarsys.2020.103457

Azaneu, M., Kerr, R., Mata, M.M., Garcia, C.A.E., Eiras Garcia, C.A. (2013). Trends in the deep Southern Ocean (1958-2010): Implications for Antarctic Bottom Water properties and volume export. Journal of Geophysical Research: Oceans, 118, 4213–4227. https://doi.org/10.1002/jgrc.20303

Boeira Dias, F., Rintoul, S. R., Richter, O., Galton-Fenzi, B. K., Zika, J. D., Pellichero, V., & Uotila, P. (2023). Sensitivity of simulated water mass transformation on the Antarctic shelf to tides, topography and model resolution. Frontiers in Marine Science, 10. https://doi:10.3389/fmars.2023.1027704

Cai, W., Santoso, A., Wang, G. et al. ENSO and greenhouse warming. Nature Clim Change 5, 849–859 (2015). https://doi.org/10.1038/nclimate2743

Clem, K. R., Renwick, J. A., McGregor, J. & Fogt, R. L. (2016). The relative influence of ENSO and SAM on Antarctic Peninsula climate. *J. Geophys. Res. Atmos.* **121**, 9324–9341.

Collares, L.L., Mata, M.M., Kerr, R., Arigony-Neto, J., Barbat, M.M. (2018). Iceberg drift and ocean circulation in the northwestern Weddell Sea, Antarctica. Deep Sea Research Part II: Topical Studies in Oceanography, 149, 10–24 https://doi.org/10.1016/j.dsr2.2018.02.014

Cook, A.J., Holland, P.R., Meredith, M.P., Murray, T., Luckman, A., Vaughan, D.G. (2016). Ocean forcing of glacier retreat in the western Antarctic Peninsula. Nature, 353, 283–287.

Costa, R.R., Ferreira, A., de Souza, M.S., Tavano, V.M., Kerr, R., Secchi, E.R., Brotas, V., Dotto, T.S., Brito, A.C., Mendes, C.R.B. (2023). Physical-biological drivers modulating phytoplankton seasonal succession along the Northern Antarctic Peninsula. Environmental Research, 231, 116273. https://doi.org/10.1016/j.envres.2023.116273

Costa, R.R., Mendes, C.R.B., Tavano, V.M., Dotto, T.S., Kerr, R., Monteiro, T., Odebrecht, C., Secchi, E.R. (2020). Dynamics of an intense diatom bloom in the Northern Antarctic Peninsula, February 2016. Limnology and Oceanography. https://doi.org/10.1002/lno.11437

Couto, N., Martinson, D.G., Kohut, J., Schofield, O., (2017). Distribution of Upper Circumpolar Deep Water on the warming continental shelf of the West Antarctic Peninsula J. Geophys. Res. Oceans, 122 https://doi.org/10.1002/2017JC012840

da Cunha, L.C., Hamacher, C., Farias, C. de O., Kerr, R., Mendes, C.R.B., Mata, M.M. (2018). Contrasting end-summer distribution of organic carbon along the Gerlache Strait, Northern Antarctic Peninsula: Bio-physical interactions. Deep Sea Research Part II: Topical Studies in Oceanography, 149, 206–217. https://doi.org/10.1016/j.dsr2.2018.03.003

Damini, B. Y., Kerr, R., Dotto, T. S., & Mata, M. M. (2022). Long-term changes on the Bransfield Strait deep 911 water masses: Variability, drivers and connections with the northwestern Weddell Sea. Deep Sea 912 Research Part I: Oceanographic Research Papers, 179, 103667. 913 https://doi.org/10.1016/j.dsr.2021.103667

Damini, B.Y., Kerr, R., Dotto, T.S., Mata, M.M. (2022). Long-term changes on the Bransfield Strait deep water masses: Variability, drivers, and connections with the

northwestern Weddell Sea. Deep Sea Research Part I: Oceanographic Research Papers, 179, 103667. https://doi.org/10.1016/j.dsr.2021.103667

Dee, D. P., Uppala, S. M., Simmons, A. J., Berrisford, P., Poli, P., Kobayashi, S., et al. (2011). The ERA-Interim reanalysis: Configuration and performance of the data assimilation system. Quarterly Journal of the Royal Meteorological Society, 137(656), 553–597. https://doi.org/10.1002/qj.828

Dotto, T.S., Kerr, R., Mata, M.M., Eiras Garcia, C.A. (2016). Multidecadal freshening and lightening in the deep waters of the Bransfield Strait, Antarctica. Journal of Geophysical Research: Oceans, 121, 3741–3756. https://doi.org/10.1002/2015JC011228

Dotto, T. S., Kerr, R., Mata, M. M., & Garcia, C. A. E. (2021). NAPv1.0: A seasonal hydrographic gridded data 939 set for the Northern Antarctic Peninsula, Southern Ocean (1.0). Zenodo. 940 https://doi.org/https://doi.org/10.5281/zenodo.4420006

Ferreira, A., Costa, R.R., Dotto, T.S., Kerr, R., Tavano, V.M., Brito, A.C., Brotas, V., Secchi, E.R., Mendes, C.R.B. (2020). Changes in phytoplankton communities along the Northern Antarctic Peninsula: Causes, impacts and research priorities. Frontiers in Marine Science, 7, 576254. https://doi.org/10.3389/fmars.2020.576254

Ferreira, M.L. de C., Kerr, R. (2017). Source water distribution and quantification of North Atlantic Deep Water and Antarctic Bottom Water in the Atlantic Ocean. Progress in Oceanography, 153, 66–83. https://doi.org/10.1016/j.pocean.2017.04.003

Fomin, L., 1964. The Dynamic Method in Oceanography. Oceanography 2, 226.

Fogt, R. L. and Marshall, G. J., (2020). The Southern Annular Mode: variability, trends, and climate impacts across the Southern Hemisphere, Wiley Interdisciplinary Reviews: Climate Change, 11, e652, https://doi.org/10.1002/wcc.652

Gomis, D., García, M.A., López, O., Pascual, A., (2002). Quasi-geostrophic 3D circulation and mass transport in the western Bransfield Strait during Austral summer 1995/96. Deep Sea Research Part II: Topical Studies in Oceanography, 49, 603–621. https://doi.org/10.1016/S0967-0645(01)00114-X

Gordey, A.S., Frey, D.I., Drozd, I.D., Krechik, V.A., Smirnova, D.A., Gladyshev, S.V., Morozov, E.G., 2024. Spatial variability of water mass transports in the Bransfield Strait based on direct current measurements. Deep Sea Research Part I: Oceanographic Research Papers, 207, 104284. https://doi.org/10.1016/J.DSR.2024.104284

Gordon, A.L., Mensch, M., Zhaoqian, D., Smethie, W.M., de Bettencourt, J., 2000. Deep and bottom water of the Bransfield Strait eastern and central basins. Journal of Geophysical Research: Oceans, 105, 11337–11346. https://doi.org/10.1029/2000JC900030

Grelowski, A., Majewick, A., Pastuszak, M., 1986. Mesoscale hydrodynamic processes in the region of Bransfield Strait and the southern part of Drake Passage during BIOMASS-SIBEX 1983/84. Polish Polar Research, 7, 353–369.

Herraiz-borreguero, L., 2020. Modified Circumpolar Deep Water intrusions in Vincennes Bay, East Modified Circumpolar Deep Water intrusions in. https://doi.org/10.1002/essoar.10504957.1

Heywood, K.J., Naveira Garabato, A.C., Stevens, D.P., Muench, R.D., 2004. On the fate of the Antarctic Slope Front and the origin of the Weddell Front. Journal of Geophysical Research: Oceans, 109. https://doi.org/10.1029/2003JC002053

Hofmann, E.E., Klinck, J.M., Lascara, C.M., Smith, D.A., 1996. Water mass distribution and circulation west of the Antarctic Peninsula and including Bransfield Strait. In: Antarctic Research Series, vol. 70, 61–80. https://doi.org/10.1029/AR070p0061

Hogg, A.M.C., Meredith, M.P., Chambers, D.P., Abrahamsen, E.P., Hughes, C.W., Morrison, A.K., 2015. Recent trends in the Southern Ocean eddy field. Journal of Geophysical Research: Oceans, 120, 257–267. https://doi.org/10.1002/2014JC010470

Huneke, W.G.C., Huhn, O., Schröeder, M., 2016. Water masses in the Bransfield Strait and adjacent seas, austral summer 2013. Polar Biology, 39, 789–798. https://doi.org/10.1007/S00300-016-1936-8

Ito, R.G., Tavano, V.M., Borges Mendes, C.R., Garcia, C.A.E., 2018. Sea-air CO2 fluxes and pCO2 variability in the Northern Antarctic Peninsula during three summer periods (2008–2010). Deep Sea Research Part II: Topical Studies in Oceanography, 149, 84–98. https://doi.org/10.1016/j.dsr2.2017.09.004

Jean-Michel, L., Eric, G., Romain, B.B., Gilles, G., Angélique, M., Marie, D., Clément, B., Mathieu, H., Olivier, L.G., Charly, R., Tony, C., Charles-Emmanuel, T., Florent, G., Giovanni, R., Mounir, B., Yann, D., Pierre-Yves, L.T., 2021. The Copernicus Global 1/12° Oceanic and Sea Ice GLORYS12 Reanalysis. Frontiers in Earth Science, 9, 698876. https://doi.org/10.3389/FEART.2021.698876

Kerr, R., Orselli, I.B.M., Lencina-Avila, J.M., Eidt, R.T., Borges Mendes, C.R., Cotrim da Cunha, L., Goyet, C., Mata, M.M., Tavano, V.M., 2017. Carbonate system properties in the Gerlache Strait, Northern Antarctic Peninsula (February 2015): I. Sea-air CO2 fluxes. Deep Sea Research Part II: Topical Studies in Oceanography, 1–11. https://doi.org/10.1016/j.dsr2.2017.07.007

Kerr, R., Mata, M.M., Mendes, C.R.B., Secchi, E.R., 2018a. Northern Antarctic Peninsula: a marine climate hotspot of rapid changes on ecosystems and ocean dynamics. Deep-Sea Research Part II: Topical Studies in Oceanography 149, 4–9. https://doi.org/10.1016/j.dsr2.2018.05.006

Kerr, R., Dotto, T.S., Mata, M.M., Hellmer, H.H., 2018b. Three decades of deep water mass investigation in the Weddell Sea (1984–2014): Temporal variability and changes. Deep Sea Research Part II: Topical Studies in Oceanography 149, 70–83. https://doi.org/10.1016/J.DSR2.2017.12.002

Kerr, R., Monteiro, T., Batista, M. S., Damini, Y. B., (2025). Physical-biological processes regulating summer sea-air CO2 exchanges along the Drake Passage and northern Antarctic Peninsula, Marine Chemistry, 269. https://doi.org/10.1016/j.marchem.2025.104497

Kim, T.W., Yang, H.W., Dutrieux, P., Wåhlin, A.K., Jenkins, A., Kim, Y.G., Ha, H.K., Kim, C.S., Cho, K.H., Park, T., Park, J., Lee, S.H., Cho, Y.K., 2021. Interannual Variation of Modified Circumpolar Deep Water in the Dotson-Getz Trough, West Antarctica. J Geophys Res Oceans 126, e2021JC017491. https://doi.org/10.1029/2021JC017491

Llanillo, P. J., Kanzow, T., Janout, M. A., & Rohardt, G. (2023). The deep-water plume in the northwestern weddell sea, Antarctica: Mean state, seasonal cycle and interannual variability influenced by climate modes. Journal of Geophysical Research: Oceans, 128(2). https://doi.org/10.1029/2022jc019375

Loeb, V.J., Hofmann, E.E., Klinck, J.M., Holm-Hansen, O., White, W.B., 2009. ENSO and variability of the Antarctic Peninsula pelagic marine ecosystem. Antarct Sci 21, 135–148. https://doi.org/10.1017/S0954102008001636

Loeb, V., Hofmann, E.E., Klinck, J.M., Holm-hansen, O., 2010. Deep-Sea Research II Hydrographic control of the marine ecosystem in the South Shetland-Elephant Island and Bransfield Strait region. Deep-Sea Research Part II 57, 519–542. https://doi.org/10.1016/j.dsr2.2009.10.004

López, O., García, M.A., Gomis, D., Rojas, P., Sospedra, J., Sánchez-Arcilla, A., 1999. Hydrographic and hydrodynamic characteristics of the eastern basin of the Bransfield Strait (Antarctica). Deep Sea Research Part I: Oceanographic Research Papers 46, 1755–1778. https://doi.org/10.1016/S0967-0637(99)00017-5

McDougall, T.; Feistel, R.; Millero, F.J.; Jackett, D.; Wright, D.; King, B.; Marion, G.; Chen, C.T.A.; Spitzer, P.; Seitz, S. The International Thermodynamic Equation of Seawater

2010 (TEOS-10): Calculation and Use of Thermodynamic Properties; Global ship-based repeat hydrography manual, IOCCP report no. 56; UNESCO: Paris, France, 2009; Volume 14.
Martínez-Moreno, J., Hogg, A. M., & England, M. H. (2022). Climatology, seasonality, and trends of spatially coherent ocean eddies. Journal of Geophysical Research: Oceans, 127(7), e2021JC017453. https://doi.org/10.1029/2021JC017453
Martinson, D. G. and McKee, D. C.: Transport of warm Upper Circumpolar Deep Water onto the western Antarctic Peninsula continental shelf. (2012), Ocean Science, 8, 433–442, https://doi.org/10.5194/os-8-433-2012
Mata, M.M., Tavano, V.M., Eiras Garcia, C.A., 2018. 15 years sailing with the Brazilian High Latitude Oceanography Group (GOAL). Deep Sea Research Part II: Topical Studies in Oceanography 149, 1–3. https://doi.org/10.1016/j.dsr2.2018.05.007
Marshall, G.J., 2003. Trends in the Southern Annular Mode from observations and reanalyses. J Clim 16, 4134–4143. https://doi.org/10.1175/1520-0442(2003)016<4134:TITSAM>2.0.CO;2
Mendes, C.R.B., Tavano, V.M., Kerr, R., Dotto, T.S., Maximiano, T., Secchi, E.R., (2018). Impact of sea ice on the structure of phytoplankton communities in the northern Antarctic Peninsula. Deep Sea Res 2 Top Stud Oceanogr 149, 111–123. https://doi.org/10.1016/j.dsr2.2017.12.003
Meredith, M.P., Hogg, A.M., 2006. Circumpolar response of Southern Ocean eddy activity to a change in the Southern Annular Mode. Geophys Res Lett 33. https://doi.org/10.1029/2006GL026499
Moffat, C., B. Owens, and R. C. Beardsley, (2009): On the characteristics of Circumpolar Deep Water Intrusions to the west Antarctic Peninsula Continental Shelf. J. *Geophysical Research*, 114, C05017, https://doi:10.1029/2008JC004955
Morrison, A.K., McC. Hogg, A., England, M.H., Spence, P., 2020. Warm Circumpolar Deep Water transport toward Antarctica driven by local dense water export in canyons. *Science Advances*, 6, eAAV2516. https://doi.org/10.1126/sciadv.aav2516
Morozov, E.G., Frey, D.I., Krechik, V.A., Polukhin, A.A., Sapozhnikov, P. V., 2021. Water Masses, Currents, and Phytoplankton in the Bransfield Strait in January 2020 55–64. https://doi.org/10.1007/978-3-030-78927-5_4
Monteiro et al. Spatiotemporal variability of dissolved inorganic macronutrients along the northern Antarctic Peninsula (1996–2019). (2023). Limnology and Oceanography, https://doi.org/10.1002/lno.12424
Miguel Andres-Martin, Cesar Azorin-Molina, Encarna Serrano, Sergi González-Herrero, Jose A. Guijarro, Shalenys Bedoya-Valestt, Eduardo Utrabo-Carazo, Sergio M. Vicente Serrano, (2024). Near-surface wind speed trends and variability over the Antarctic Peninsula, 1979–2022, Atmospheric Research, https://doi.org/10.1016/j.atmosres.2024.107568.
Mukhametyanov, R. Z., Frei. D.I., Morozov, E.G., 2022. Currents in the Bransfield Strait Based on Geostrophic Calculations and Data of Instrumental Measurements, *Izvestiya, Atmospheric and Oceanic Physics*. https://doi.org/10.1134/S0001433822050061
Niller, P.P., Amos, A., Hu, J.H., 1991. Water masses and 200 m relative geostrophic circulation in the western Bransfield Strait region. Deep Sea Research Part A, Oceanographic Research Papers 38, 943–959. https://doi.org/10.1016/0198-0149(91)90091-S
Oelerich, R., Heywood, K.J., Damerell, G.M., Thompson, A.F., 2022. Wind-Induced Variability of Warm Water on the Southern Bellingshausen Sea Continental Shelf. J Geophys Res Oceans 127, e2022JC018636. https://doi.org/10.1029/2022JC018636

Ong E. Q. Y., Doddridge E., Andrew McC. Hogg, et al. Seasonal sea-ice and eddy variability around the Antarctic margin. ESS Open Archive. December 27, 2024. https://doi.org/10.22541/essoar.173532505.52665007/v1

Orsi, A.H., Whitworth, T., Nowlin, W.D., 1995. On the meridional extent and fronts of the Antarctic Circumpolar Current. Deep-Sea Research Part I 42, 641–673. https://doi.org/10.1016/0967-0637(95)00021-W

Renner, A.H.H., Thorpe, S.E., Heywood, K.J., Murphy, E.J., Watkins, J.L., Meredith, M.P., 2012. Deep-Sea Research I Advective pathways near the tip of the Antarctic Peninsula : Trends, variability, and ecosystem implications. Deep-Sea Research Part I 63, 91–101. https://doi.org/10.1016/j.dsr.2012.01.009

Ruiz Barlett, E.M., Tosonotto, G. V, Piola, A.R., Sierra, M.E., Mata, M.M., 2018. On the temporal variability of intermediate and deep waters in the Western Basin of the Bransfield Strait. Deep Sea Research Part II: Topical Studies in Oceanography 149, 31–46. https://doi.org/10.1016/j.dsr2.2017.12.010

Rott, H., Abdel Jaber, W., Wuite, J., Scheiblauer. S., Floricioiu, D., and Nagler, T.: Digital data on coastlines, surface velocities and surface elevation change of Larsen A abd B glaciers, 2011 to 2016. (2018). http://cryoportal.enveo.at/data/samba/

Sanchez, N., Reiss, C.S., Holm-Hansen, O., Hewes, C.D., Bizsel, K.C., Ardelan, M.V., 2019. Weddell-Scotia Confluence effect on the iron distribution in waters surrounding the South Shetland (Antarctic Peninsula) and South Orkney (Scotia Sea) Islands during the austral summer in 2007 and 2008. *Frontiers in Marine Science*, 6, 771. https://doi.org/10.3389/fmars.2019.00771

Sangrà, P., Gordo, C., Hernández-Arencibia, M., Marrero-Díaz, Á., Rodríguez-Santana, A., Stegner, A., Martínez-Marrero, A., Pelegrí, J.L., Pichon, T., 2011. The Bransfield current system. Deep Sea Research Part I: Oceanographic Research Papers 58, 390–402. https://doi.org/10.1016/j.dsr.2011.01.011

Sangrà, P., Stegner, A., Hernández-Arencibia, M., Marrero-Díaz, Á., Salinas, C., Aguiar-González, B., Henríquez-Pastene, C., Mouriño-Carballido, B., 2017. The Bransfield Gravity Current. Deep Sea Research Part I: Oceanographic Research Papers 119, 1–15. https://doi.org/10.1016/J.DSR.2016.11.003

Santos-Andrade, M., Kerr, R., Orselli, I.B.M., Monteiro, T., Mata, M.M., Goyet, C., 2023. Drivers of Marine CO2-Carbonate Chemistry in the Northern Antarctic Peninsula. Global Biogeochem Cycles 37, e2022GB007518. https://doi.org/10.1029/2022GB007518

Schloss, I.R., Ferreyra, G.A., Ferrario, M.E., Almandoz, G.O., Codina, R., Bianchi, A.A., Balestrini, C.F., Ochoa, H.A., Pino, D.R., Poisson, A., 2007. Role of plankton communities in sea–air variations in pCO2 in the SW Atlantic Ocean. Mar Ecol Prog Ser 332, 93–106. https://doi.org/10.3354/MEPS332093

Thompson, A.F., Heywood, K.J., Thorpe, S.E., Renner, A.H.H., Trasviña, A., 2009. Surface Circulation at the Tip of the Antarctic Peninsula from Drifters. J Phys Oceanogr 39, 3–26. https://doi.org/10.1175/2008JPO3995.1

Thompson, D. W. J., Solomon, S., Interpretation of Recent Southern Hemisphere Climate Change. (2002). Science, 296.

Trasviña, A., Heywood, K.J., Renner, A.H.H., Thorpe, S.E., Thompson, A.F., Zamudio, L., 2011. The impact of high-frequency current variability on dispersion off the eastern Antarctic Peninsula. J Geophys Res Oceans 116. https://doi.org/10.1029/2011JC007003

van Caspel, M., Hellmer, H.H., Mata, M.M., van Caspel, M., Hellmer, H.H., Mata, M.M., 2018. On the ventilation of Bransfield Strait deep basins. Deep Sea Res 2 Top Stud Oceanogr 149, 25–30. https://doi.org/10.1016/j.dsr2.2017.09.006

Veny, M., Aguiar-González, B., Marrero-Díaz, Á., Rodríguez-Santana, Á., 2022. Seasonal circulation and volume transport of the Bransfield Current. PrOce 204, 102795. https://doi.org/10.1016/J.POCEAN.2022.102795

Veny, M., Aguiar-González, B., Marrero-Díaz, Á., Pereira-Vázquez, T., Rodríguez-Santana, Á., 2024. Biophysical coupling of seasonal chlorophyll-a bloom variations and phytoplankton assemblages across the Peninsula Front in the Bransfield Strait. Ocean Science 20, 389–415. https://doi.org/10.5194/OS-20-389-2024

Von Gyldenfeldt, A.B., Fahrbach, E., García, M.A., Schröder, M., 2002. Flow variability at the tip of the Antarctic Peninsula. Deep Sea Research Part II: Topical Studies in Oceanography 49, 4743–4766. https://doi.org/10.1016/S0967-0645(02)00157-1

Wang, X., Moffat, C., Dinniman, M.S., Klinck, J.M., Sutherland, D.A., Aguiar-González, B., 2022. Variability and Dynamics of Along-Shore Exchange on the West Antarctic Peninsula (WAP) Continental Shelf. J Geophys Res Oceans 127, e2021JC017645. https://doi.org/10.1029/2021JC017645

Wessel, P., Smith, W.H.F., 1996. A global, self-consistent, hierarchical, high-resolution shoreline database. J Geophys Res Solid Earth 101, 8741–8743. https://doi.org/10.1029/96JB00104

Wilson, C., Klinkhammer, G.P., Chin, C.S., 1999. Hydrography within the Central and East Basins of the Bransfield Strait, Antarctica. J Phys Oceanogr 29, 465–479. https://doi.org/10.1175/1520-0485(1999)029<0465:HWTCAE>2.0.CO;2

Yamazaki, K. et al. (2021). Multidecadal poleward shift of the southern boundary of the Antarctic Circumpolar Current off East Antarctica. *Sci. Adv.* **7**, https://doi.org/10.1126/sciadv.abf8755

Yuan X. ENSO-related impacts on Antarctic sea ice: a synthesis of phenomenon and mechanisms. Antarctic Science. 2004;16(4):415-425. doi:10.1017/S0954102004002238

Zhou, M., Niiler, P.P., Hu, J.H., 2002. Surface currents in the Bransfield and Gerlache Straits, Antarctica. Deep Sea Research Part I: Oceanographic Research Papers 49, 267–280. https://doi.org/10.1016/S0967-0637(01)00062-0

Zhou, M., Niiler, P.P., Zhu, Y., Dorland, R.D., 2006. The western boundary current in the Bransfield Strait, Antarctica. Deep Sea Research Part I: Oceanographic Research Papers 53, 1244–1252. https://doi.org/10.1016/J.DSR.2006.04.003